

WALLABY Pilot Survey: the Tully-Fisher relation in the NGC 4808, Vela and NGC 5044 fields

Jeremy Mould,^{1,2*} T. H. Jarrett,³ Hélène Courtois⁴ Albert Bosma⁵ Nathan Deg¹⁴ Alexandra Dupuy⁸ Lister Staveley-Smith^{9,10} E.N. Taylor¹ Jayanne English²⁰ S. H. A. Rajohnson²¹ Renée Kraan-Korteweg²¹ Duncan Forbes¹ Helga Dénes⁷ Karen Lee-Waddell^{6,9,10} Austin Shen^{18,19} O. I. Wong^{6,9,16} Benne Holwerda¹³ Bärbel Koribalski^{11,12} Denis Leahy²² Pavel Mancera Piña¹⁵ Niankun Yu^{17,23}

¹Centre for Astrophysics & Supercomputing, Swinburne University, Hawthorn, VIC 3122, Australia.

²ARC Centre of Excellence for Dark Matter Particle Physics

³Astronomy Department, University of Cape Town, Private Bag X3, Rondebosch 7701, South Africa

⁴UCB Lyon 1, IUF IP21, Lyon, 69622, Villeurbanne, France.

⁵Aix Marseille University, CNRS, CNES, LAM Marseille, France.

⁶CSIRO Space & Astronomy, PO Box 1130, Bentley, WA 6102, Australia.

⁷School of Physical Science & Nanotechnology, Yachay Tech University, Hacienda San José S/N 100119, Urcuquí, Ecuador.

⁸Korea Institute for Advanced Study, 85, Hoegi-ro, Dongdaemun-gu, Seoul 02455, Republic of Korea.

⁹ICRAR-M468, University of Western Australia, 35 Stirling Highway, Crawley, WA 6009, Australia.

¹⁰ICRAR - Curtin University, Bentley, WA 6102, Australia.

¹¹Australia Telescope National Facility, CSIRO Astronomy & Space Science, PO Box 76, Epping, NSW 1710, Australia.

¹²School of Science, Western Sydney University, Locked Bag 1797, Penrith, NSW 2751, Australia.

¹³University of Louisville, Department of Physics & Astronomy, Louisville KY 40292, USA.

¹⁴Department of Physics, Engineering Physics & Astronomy, Queen's University, Kingston, ON, K7L 3N6, Canada.

¹⁵Leiden Observatory, Leiden University, P.O. Box 9513, 2300 RA Leiden, The Netherlands

¹⁶ARC Centre of Excellence for All Sky Astrophysics in 3 Dimensions (ASTRO 3D).

¹⁷National Astronomical Observatories, Chinese Academy of Sciences, Beijing, 100101, P.R. China

¹⁸CSIRO Space & Astronomy, PO Box 1130, Bentley, WA 6102, Australia

¹⁹Australian SKA Regional Centre (AusSRC)

²⁰Department of Physics and Astronomy, University of Manitoba, Winnipeg, Manitoba, Canada, R3T 2N2, Canada

²¹Department of Astronomy, University of Cape Town, Private Bag X3, Rondebosch 7701, South Africa

²²Department of Physics and Astronomy, University of Calgary, Calgary, AB T2N 1N4, Canada

²³Key Laboratory of Radio Astronomy and Technology, Chinese Academy of Sciences, Beijing, 100101, P.R. China

Accepted 2024 June 14. Received 2024 June 13; in original form 2024 May 8

ABSTRACT

The Tully-Fisher Relation (TFR) is a well-known empirical relationship between the luminosity of a spiral galaxy and its circular velocity, allowing us to estimate redshift independent distances. Here we use high signal-to-noise HI 21-cm integrated spectra from the second pilot data release (PDR2, 180 deg²) of the Widefield ASKAP L-band Legacy All-sky Blind survey (WALLABY). In order to prepare for the full WALLABY survey, we have investigated the TFR in phase 2 of the pilot survey with a further three fields. The data were obtained with wide-field Phased Array Feeds on the Australian Square Kilometre Array Pathfinder (ASKAP) and have an angular resolution of 30 arcsec and a velocity resolution of ~ 4 km s⁻¹. Galaxy luminosities have been measured from the Wide-field Infrared Survey Explorer (WISE), and optical galaxy inclinations from the Dark Energy Camera Legacy Survey. We present TFRs for wavelengths from 0.8–3.4 μ m. We examine sources of galaxy inclination data and investigate magnitudes from the DECam Local Volume Exploration Survey (DELVE) and DENIS catalogues and the 4HS target catalogue based on the VISTA Hemisphere Survey (VHS). We consider the baryonic TFR. These are all of interest for TFR using the full WALLABY survey of 200,000 galaxies. We demonstrate that WALLABY TFR distances can take their place among state of the art studies of the local velocity field.

Key words: large scale structure of the Universe, surveys, infrared photometry, radio astronomy

1 INTRODUCTION

In the local Universe large-scale structure can be investigated using redshift- independent distance indicators, such as the

* E-mail: jmould@swin.edu.au

Tully-Fisher Relation (TFR), which allow galaxies' peculiar velocities to be measured. Peculiar velocities come about because mass density inhomogeneities in the Universe act on galaxies and perturb the velocities given to them by the expansion of the Universe. To be exact, the peculiar velocity of a galaxy arises from the volume integral of the overdensities divided by the square of the distances to them, multiplied by the growth rate. Here the over-density is $\delta = \delta\rho/\bar{\rho} - 1$ where ρ and $\bar{\rho}$ are the density and mean density of the Universe, and the growth rate, f , is approximately $\Omega_m^{4/7}$ in the Λ CDM standard model, where Ω_m is the mass density parameter. Peculiar velocities have therefore been used to constrain the cosmological parameter $f\sigma_8$ (σ_8 is the amplitude of the power spectrum on scales of $8h^{-1}$ Mpc; Adams & Blake 2017; Dupuy et al. 2019), thus providing a test of gravity on very large scales. To measure peculiar velocities we need redshift-independent distance indicators, such as the Fundamental Plane (Djorgovski & Davis 1987), the supernova standard candle (Kowal 1968) and the Tully-Fisher relation (Tully & Fisher 1977).

The Widefield ASKAP L-band Legacy All-sky Blind survey (or WALLABY; Koribalski et al. 2020) is being conducted on the Australian SKA Pathfinder (ASKAP, Hotan et al. 2021), an innovative imaging radio telescope located at the Murchison Radio-astronomy Observatory in Western Australia. The aim of WALLABY is to use the powerful wide-field phased-array technology of ASKAP to observe initially 14,000 square degrees of the southern hemisphere in the 21-cm line of neutral hydrogen at 30-arcsec resolution (Westmeier et al. 2022)¹. The survey began in January 2023, but a number of fields were observed in 2022 as a pilot program, among them the phase 2 target fields centred on NGC 4808, Vela and NGC 5044. WALLABY pilot survey phase 2 data were released in DR2 by Murugesan et al. (2024).

The goals of this paper are first to learn as much as possible about the Tully-Fisher Relation (TFR) early on, since the full WALLABY Survey will be a hundred times larger than the pilot survey, and, second, to measure peculiar velocities to be compared with expectations from the CosmicFlows program (Courtois & Tully 2015).

In the paper we extract and measure HI spectra of galaxies in these fields and combine them (§§2,3 & 4) with customized WISE total magnitudes (Jarrett et al. 2023). Infrared photometry has the advantage of being less affected by extinction in our Galaxy and the target galaxies (Aaronson, Huchra & Mould 1979). We also investigate available I band photometry and optical diameters. The utility of WALLABY for peculiar velocity measurement is considered in §5, and our conclusions are summarized in §6.

2 THE NGC 4808 FIELD

Source finding using SoFiA (Westmeier et al. 2021; Serra et al. 2015) and HI measurements for the NGC 4808 field follow Courtois et al. (2022; Paper 1). SoFiA2 uses the Smooth + Clip algorithm for source finding, which operates by spatially and spectrally smoothing the data on multiple scales

and applying a user-defined flux threshold relative to the noise level in each iteration. A wide range of useful preconditioning and post-processing filters is available, including noise normalization, flagging of artifacts and reliability filtering. Values of W_{50} were measured directly from the flux density versus frequency spectra produced by the WALLABY pipeline. All sources were inspected by Tobias Westmeier, and objects deemed to be questionable were deleted. An example would be an optical galaxy split in two by SoFiA. Over the 3 fields between 7 and 14% of the sources were eliminated in this way. Half of these involve pairs or splits. It is customary to exclude such objects from the TFR. The effects of radio frequency interference are also trapped at this stage.

Table 1 reports the TFR data for the NGC 4808 field. Column (1) is the name of the WALLABY survey HI detection. Columns (2) & (3) are the SoFiA coordinates of the WALLABY HI detections. Column (4) is the mean velocity of the HI profile integrated over the spectrum. Column (5) is the axial ratio of the DECaLS² g band galaxy image, which yields the inclination i of the disk. The axial ratio was measured at approximately 5% of the sky background level with the ellipse task of IRAF³. A minimum axial ratio of 0.2 was adopted. Zeros denote galaxies for which no axial ratio could be measured.

Coordinates from the HyperLeda catalogue differ from WALLABY coordinates by $7.5''$ rms after 2.5σ deviates were removed, with equal contributions from RA and Dec. The WALLABY beam diameter is $30''$ and this is a contributor⁴. In some cases there may also be a difference between the HI centroid and the centroid of the stellar light. Columns (6) & (7) are the WISE⁵ W1 total galaxy magnitude after removal of contaminating stars and its uncertainty. Columns (8) & (9) are the width at half peak (or double peak) of the HI profile and its uncertainty. Column (10) is the signal to noise ratio of the HI profile. Column (11) provides other names for the source from the HyperLeda catalogue. Double identifications were eliminated by choosing the closer of the two galaxies. In the TFR we use W_{mx} , the width after correction for resolution and turbulence following Tully & Fouqué (1985). The velocity axis of the TFR is $\Delta V(0) = W_{mx} / \sin i / (1+z)$, where i is obtained from column (5)'s optical axial ratio. Nineteen galaxies have W_{mx} both measured from WALLABY and compiled by Tully et al. (2009, EDD, the Extragalactic Distance Database) and Courtois et al. (2009). The mean velocity width ratio, EDD/WALLABY, is 1.00 ± 0.01 , and the χ^2 per degree of freedom for the identity relation is 0.27, indicating that for these bright galaxies the velocity width uncertainties have been overestimated. The velocity structure of the NGC4808 field is shown in Figure 1. Some groups and filaments of galaxies are visible.

² <https://datalab.noirlab.edu/ls/decals.php>

³ <https://iraf-community.github.io>

⁴ Typical position uncertainties for HI point sources in WALLABY are estimated as the beam diameter ($30''$) divided by the source signal-to-noise, resulting in $7.5''$ uncertainty only for 4σ detections. Westmeier et al. (2022) found an rms of $5''$ in the phase 1 pilot survey

⁵ Wright et al. (2010)

¹ Sky coverage is described at <https://wallaby-survey.org/overview/>

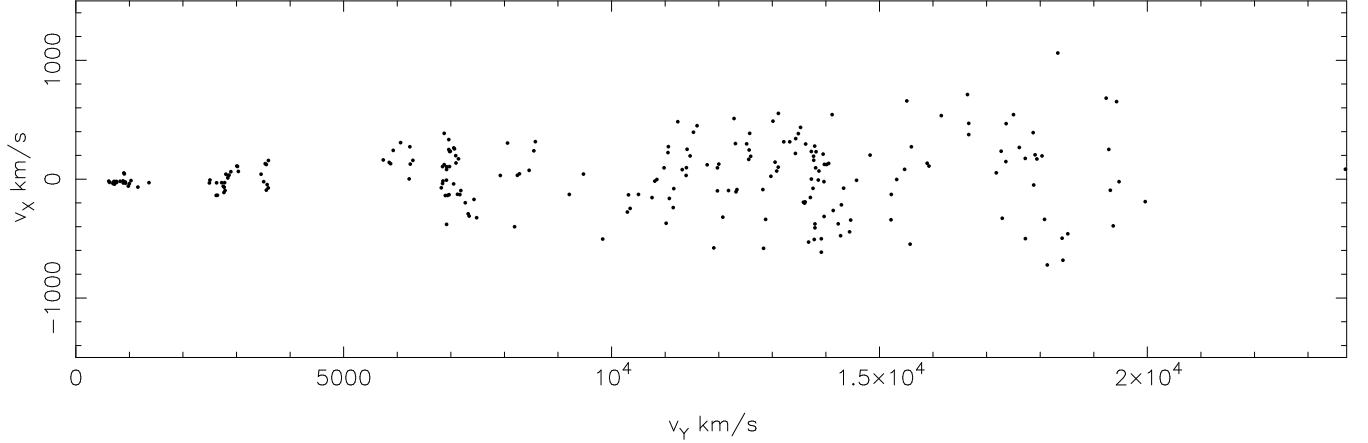


Figure 1. WALLABY galaxies in the NGC4808 field in the supergalactic plane. The long axis is the heliocentric recession velocity in the SGY direction, and the vertical axis is the the heliocentric recession velocity in the SGX direction. The structure is evident in galaxy groups and filaments.

2.1 Comparison with Arecibo observations

Only a small portion of the WALLABY footprint protrudes into the northern hemisphere. The NGC 4808 field therefore provides a rare opportunity to compare observations with those obtained by the Arecibo Observatory in the ALFALFA Survey (Haynes et al. 2018) and catalogued in EDD and labelled Wmx1. Figure 2 shows this comparison.

The measured redshifts of WALLABY and Arecibo are in good agreement. Although 6% of the velocity widths are in disagreement by more than twice the joint uncertainty, this is no more than expected statistically. We note the more extreme cases, WALLABY J125258+073025, WALLABY J130412+43057, WALLABY J130012+054417 and WALLABY J130950+062601. Examination of the HI profiles of the discrepant galaxies reveals that both their WALLABY and ALFALFA profiles are of low signal to noise (S/N) and they are all distant, $cz > 10,000 \text{ km s}^{-1}$. Another way of looking at this comparison is in the lower section of Figure 2. Here the *hyperfit* slope is significant, -0.072 ± 0.006 .

2.2 TFR for the NGC 4808 field

The galaxy inclinations are calculated in the normal way

$$\cos^2 i = \frac{(b/a)^2 - 0.2^2}{1 - 0.2^2} \quad (1).$$

where b/a is the axial ratio. The minimum axial ratio of 0.2 has been adopted since the original work of Tully & Fisher (1977). Paturel et al. (2003) listed no galaxies with $b/a < 0.25$ in their Principal Galaxies Catalogue. In §A4 we note that we see exceptions with $b/a < 0.2$, but these are recorded in Table 1 as $b/a = 0.2$. This is not an issue, as they are clearly edge-on. We use the data of Table 1 to construct the TFR. Excluded from Figure 3 are galaxies with inclinations less than 45° for which $\sin i$ is too uncertain, those with velocity width errors greater than 20 km s^{-1} , and those with $S/N < 3.7$. Absolute magnitudes were calculated with a Hubble

Constant of $73 \text{ km s}^{-1} \text{ Mpc}^{-1}$ (Riess et al. 2022) after correction of heliocentric velocities to the cosmic microwave background frame, following Lineweaver et al. (1996). A simple least squares linear fit to Figure 3, excluding the outlier WALLABY J130436+045341 and 3 other 2.5σ deviates, gives a χ^2 per degree of freedom of 5.1, its difference from unity indicating that the velocity width uncertainties are partially responsible for the scatter in the TFR, but there is intrinsic scatter as well. In §4.2 we quantify the uncertainties in i which contribute 0.53 mag to the vertical errors, compared with 0.46 mag for the width uncertainties here. By comparison errors in W1 are negligible, growing slowly from 0.01 to 0.1 mag going from 14 to 17 mag in W1. We explore possible ways to reduce the uncertainties in i in the Appendix. A similar χ^2 is obtained from a fit with the *hyperfit* Bayesian regression package (Robotham & Obreschkow 2015), including an assumed Gaussian scatter of 200 km/s from peculiar velocities. *Hyperfit* maximizes the likelihood of a linear fit in the presence of uncertainties in both coordinates. This is an important distinction from a least squares fit, when there is a range of errors in the data. Unbiased estimators for the population model of the vertical scatter and its variance can be obtained. The website interface to *Hyperfit* was accessed at hyperfit.icrar.org. The intrinsic scatter in the TFR measured by *hyperfit* is 0.85 mag. Selection biases may also affect the fit, but these are not investigated here

Photometry for galaxies with names in column (11) of Table 1 is also available from the Siena Galaxy Atlas (Moustakas et al. 2023). This is presented in the Appendix.

2.3 Star formation

The W1 WISE bandpass has some sensitivity to PAH emission (Cluver et al. 2017) and so we have examined the W1–W2 colour in this sample. Figure 4 shows that the vast majority of these HI detections has $W1-W2 < 0.2$ mag, making it unlikely that there is a significant number of starburst

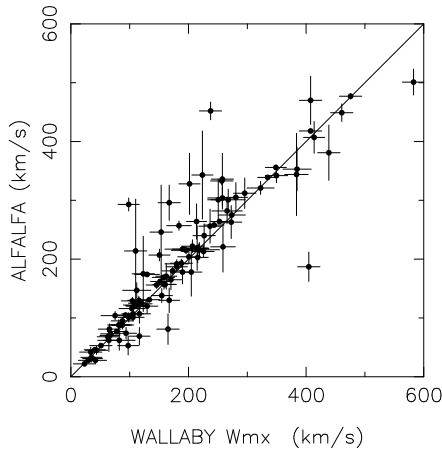


Figure 2. (a) Comparisons of velocity widths from Table 1 and those from ALFALFA.

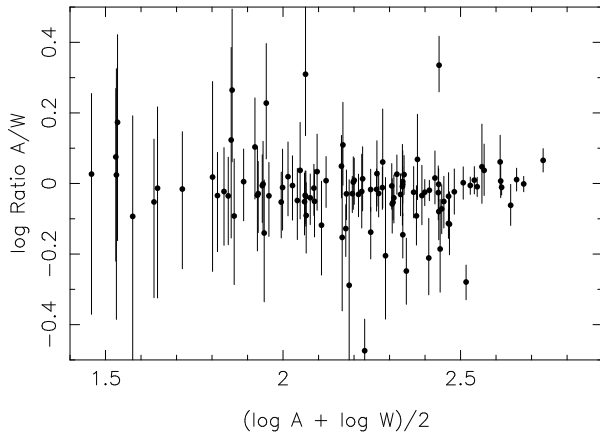


Figure 2. (b) $A = \text{ALFALFA}$, $W = \text{WALLABY}$. The vertical axis essentially shows the difference between WALLABY and ALFALFA velocity widths.

galaxies in the sample. We have located galaxies with $W1-W2 > 0.25$ mag in the TFR of Figure 3 and only one of them, WALLABY J130903+065753 is significantly discrepant in the TFR (on the high luminosity side.) It may be a starburst galaxy.

2.4 Baryonic TFR

For galaxies with a large HI mass relative to their stellar mass it stands to reason that adding it to the stellar mass will make a good alternative TFR (McGaugh et al. 2000). For our sample the HI mass is a product of the template

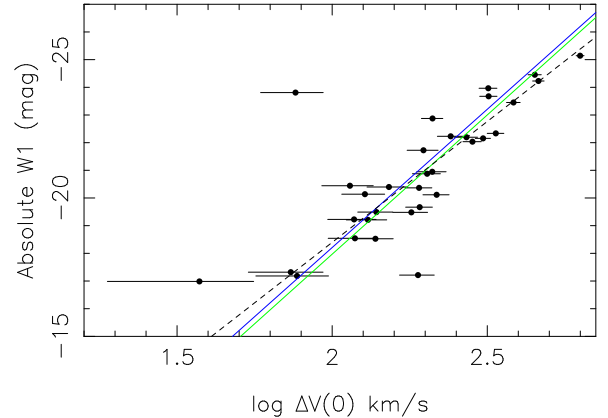


Figure 3. TFR for the NGC4808 field. The dashed line is the best unweighted linear fit; the green line is the result from *hyperfit*, which weights the fitted points by their uncertainties and allows for intrinsic scatter. The blue line is the TFR of Bell et al. (2023).

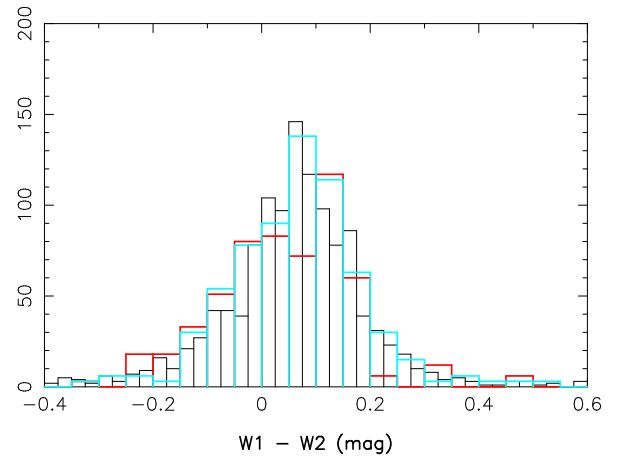


Figure 4. Distribution of $W1-W2$ colours for the galaxies in Table 1 (blue). The Vela and NGC 5044 fields are shown in red and black respectively. Vela and NGC 4808 have been upscaled by a factor of 3 for ease of comparison

science code⁶ run after the SoFia pipeline and correction for the WALLABY flux deficit, and the stellar mass in solar masses can be calculated from

$$\log M_* = -0.04 + 1.12 \log L_{W1} \quad (2)$$

(Wen et al. 2013), where L_{W1} is the 3.4μ luminosity in solar units. We also considered the stellar mass formula of Cluver et al. (2014). That formula gives a stellar mass larger by a

⁶ carnaby.aussrc.org/mnt/shared/wallaby/notebooks/WALLABY_notebooks/user_science.ipynb

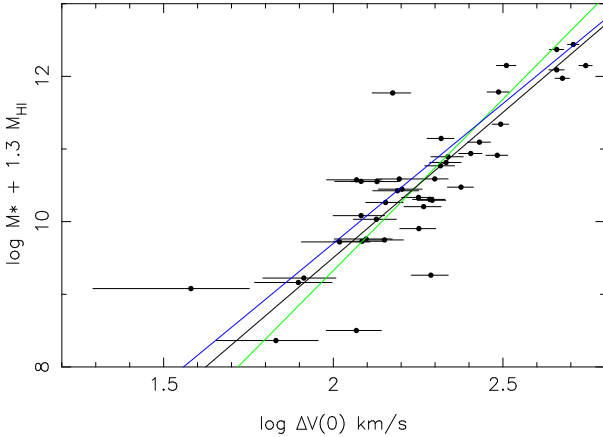


Figure 5. Baryonic TFR for galaxies in the NGC 4808 field with $cz < 10,000 \text{ km s}^{-1}$. The vertical axis is the sum of stellar and gas masses. The black line has slope 4. The green line is the *hyperfit* with slope 4.45 ± 0.29 . The blue line is from Lelli et al. (2019).

factor 1.42 ± 0.02 than Wen’s, and we have not used it because the uncertainties in WISE W2 are 50% larger than in W1⁷. The HI mass is multiplied by 1.3 to account approximately for other species (McGaugh et al. 2021), and corrected to the H_0 value used for M_* . Figure 5 is the baryonic TFR for galaxies with $cz < 10,000 \text{ km s}^{-1}$. With four 2.5σ deviates removed, the scatter about the linear least squares fit and about the *hyperfit* is 0.25 dex or $0.63 \pm 0.14 \text{ mag}$, compared with $0.65 \pm 0.13 \text{ mag}$ for the W1 TFR. Although the baryonic TFR is an alternative to the W1 TFR, it seems to be equal, rather than superior, for the purposes of measuring peculiar velocities.

3 TFR FOR THE VELA FIELD

Table 2 contains the optical, infrared and radio data for the Vela field, centred on $10^h 3^m$ and $-45^d 36^m$, and has the same format as Table 1. The structure of this field is shown in Figure 6, strengthened by redshifts from the overlapping region of the MeerKAT Vela supercluster survey (Rajohnson et al. (2024), and the TFR for the field with $S/N > 3$ is shown in Fig 7. We dropped the S/N threshold from that used in the previous field because of the smaller number of galaxies available. The vertical scatter for a linear fit excluding the lowest velocity width galaxy WALLABY J095710-485624, which is an outlier, is 0.86 mag. Although the Vela field is at low Galactic latitude (-8°), it proved possible to measure accurate W1 total magnitudes by removing superposed stars. The field is close to the centre of the Laniakea Supercluster (Tully et al. 2014), and will be of importance in the study of the velocity field in this region. We defer this to a future study when adjacent fields can be included.

⁷ The procedure described in the Appendix makes this choice moot in the use of the BTFR for CosmicFlows4.

4 THE NGC 5044 FIELD

This field is the largest of the pilot survey at 120 square degrees. Its structure is shown in Figure 8. The WALLABY and WISE data are in Table 3, which has the same format as Table 1, and the TFR is Figure 9. Where the galaxy seemed too round to warrant ellipse fitting, a zero appears in the axial ratio column of Table 3. Zeros were also recorded in the fairly rare case that the source was just outside the boundaries of the closest DECaLS image. Comparison with published data from Nancay, Greenbank and Parkes (Tully et al. 2009, EDD, Springob et al. 2005, Theureau et al. 2006, and Koribalski et al. 2004) is in Tables 4 and 5 and Figures 10 and 11, which compare WALLABY velocities with published velocities and WALLABY velocity widths with published velocity widths, respectively. Where there are two published HI profiles, both are plotted in the figures. The last two columns of these tables are the WALLABY values from Table 3. The comparison is good. With the 3 most deviant points in Figure 11 removed, there is an offset of $2 \pm 2 \text{ km s}^{-1}$ from the dashed line. The velocity widths in Tables 4 & 5 and Figures 10 & 11 have not been corrected for resolution and turbulence. The fitted TFRs in our three WALLABY fields are similar to one another within the errors.

Fu (2024) has developed a Lucy rectification algorithm for cases where axial ratios are highly uncertain, which produces a TFR based on the statistical distribution of galaxy inclinations. We applied this algorithm to the NGC 5044 field, as it offered by far the largest sample. One starts with an initial un-inclination-corrected (M_{W1} , W_{50}) plane, and the algorithm then converges and reduces the scatter. However, the scatter in the final statistical TFR obtained was 1.79 mag rms, compared with 1.08 mag in Figure 9 with the $\sin i$ term included. Although it would save a lot of painstaking measurements with uncertainties that are not well characterized, we elected not to use this algorithm. Axial ratio information is valuable for WALLABY TFR data.

4.1 HyperLeda diameters

The Principal Galaxies Catalogue (Paturel et al. 1992, PGC) is a very good match to WALLABY source lists with 1173 out of 1672 sources with PGC or other bright galaxy names in Tables 1–3 (70%). Paturel et al. (2003) have measured diameters and axis ratios on the RC2 system (de Vaucouleurs et al. 1976) at a limiting surface brightness of 25 B magnitudes per arcsec². A related 21 cm galaxy scaling relation to the TFR is that between diameter and velocity width. PGC galaxies have D_{25} and R_{25} in HyperLeda (Makarov et al. 2014), and so the diameters can be corrected to uniform face-on surface brightness by a prescription in the RC2. For a Hubble Constant of $73 \text{ km s}^{-1} \text{ Mpc}^{-1}$ the relation is shown in Figure 12. The scatter in the relation is 0.18 dex, which is equivalent to 0.9 mag in the standard candle version of the TFR, since $\delta d/d = (\ln 10)\delta \log D$, where d is distance and D is diameter, whereas $2\delta d/d = 0.4(\ln 10)\delta m$, where m is magnitude. Nevertheless, the diameter relation is competitive in this context, and opens the possibility of using both luminosity and diameter information along with velocity width. That would be analogous to the Fundamental Plane for early-type galaxies. *Hyperfit* reports a significant correlation between diameter and axial ratio uncertainty, in

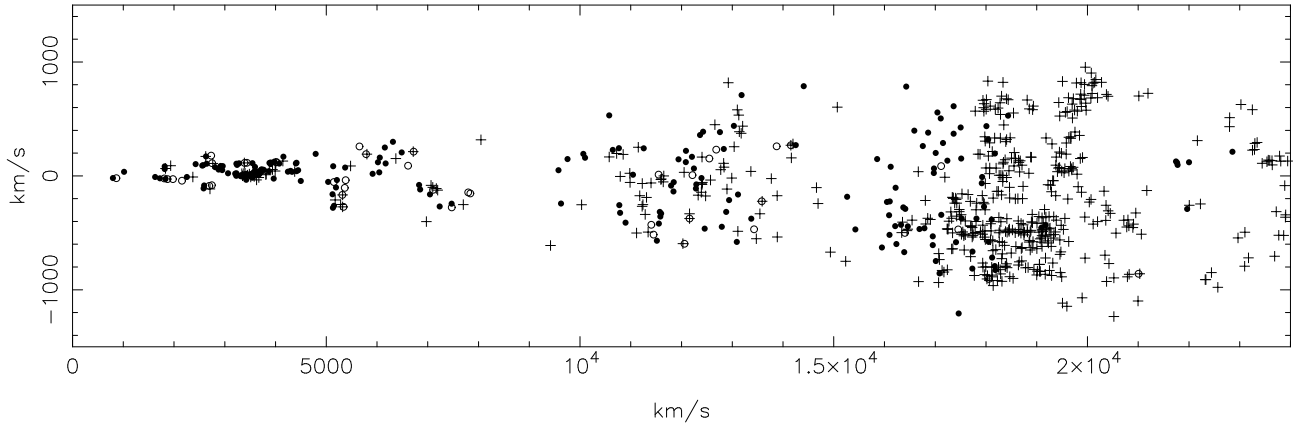


Figure 6. WALLABY Vela galaxies in the supergalactic plane. The long axis is the heliocentric recession velocity in the SGY direction, the vertical axis, the SGX direction. The dynamically significant Vela Supercluster identified by Kraan-Korteweg et al. (2017) and Courtois et al. (2019) is visible at $18,000 \text{ km s}^{-1}$ within WALLABY’s range. Redshifts from Table 2 are solid symbols, MeerKAT redshifts (Rajohnson et al. 2024) are open symbols and published and forthcoming optical Vela redshifts are plus signs.

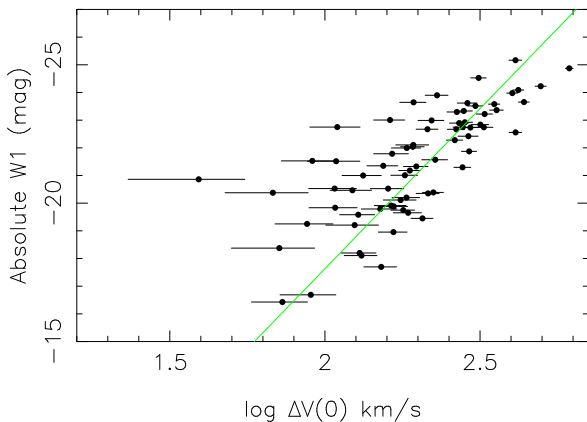


Figure 7. TFR for the Vela field. The green line is the *hyperfit*.

the sense that the largest physical diameter galaxies have 0.14 larger R_{25} uncertainties than those ten times smaller, but this would not⁸ seem to act to suppress the scatter in Figure 12. If the luminosity TFR and the diameter TFR are used jointly as they stand, however, errors in velocity width and inclination will produce errors in distance that correlate.

⁸ A change of 0.14 in R_{25} of 0.14 only makes a difference of 2 degrees in inclination on average.

4.2 Kinematic inclinations

Deg et al. (2022) and Murugesan et al. (2024) have made kinematic maps, including rotation curves, of many WALLABY galaxies, 108 of which are in the present work. In this work the inclinations of two flat disk models (FAT and 3DBAROLO) are averaged together and the uncertainty is set to half the difference between the two fits. In the flat disk algorithm geometric parameters are averaged across all radii. We have matched those with the galaxies in Tables 1–3 and the comparison of inclinations is shown in Figure 13. The solid correlation gives us confidence in our ellipse fitted axial ratios. There is also a good correlation between the axial ratios in Table 3 and HyperLeda axial ratios (Figure 14). If we assume the inclinations derived from Table 3 have an uncertainty of 12.5 degrees, we obtain $\chi^2 = 1$ in a 1:1 fit. There is no significant offset between kinematic and axial ratio inclinations down to the 1 degree level. Further discussion of axial ratios is in the Appendix.

4.3 I and J magnitudes

An additional resource is the DECam Local Volume Exploration Survey (DELVE DR2 catalog, Drlica-Wagner et al. 2022). We explore this because W1 total magnitudes may not be available for the volume of data generated by the full WALLABY survey. To reduce multiple matching, PGC positions were used, and cuts were made to SExtractor parameters (Bertin & Arnouts 1999) semi-major axis (> 5 arcsec), g magnitude (< 19) and positional error < 15 arcsec. Where multiple matching occurred, the closest galaxy to the PGC position was taken to be the match. Inspection of the DECaLS images confirmed that this is an effective procedure in finding the galaxy that is most likely to be the HI source. A TFR is shown in Figure 15, where the i mag-

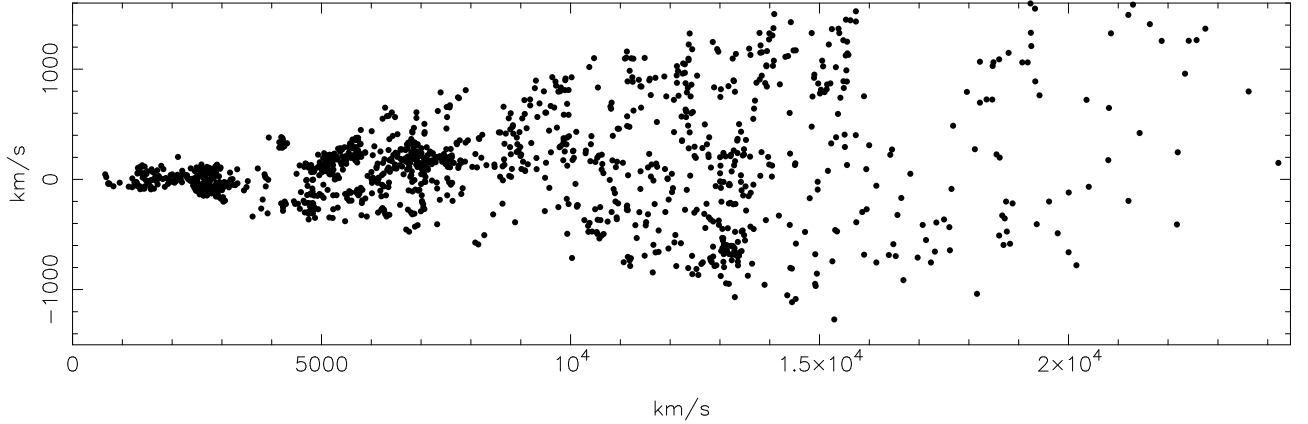


Figure 8. WALLABY galaxies from the NGC 5044 field in the supergalactic plane. The long axis is the heliocentric recession velocity in the SGY direction. The vertical axis is the SGX coordinate.

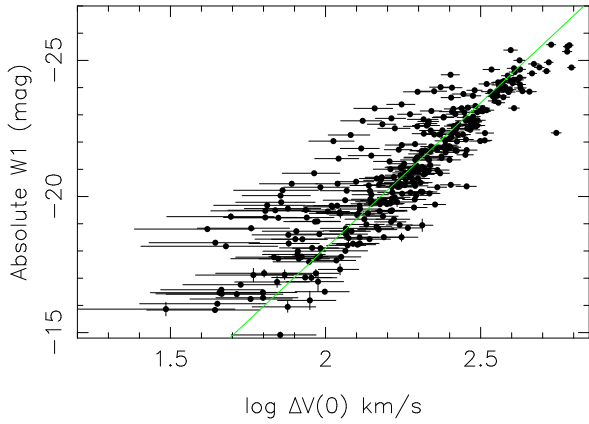


Figure 9. TFR for the NGC5044 field. Fourteen 3σ deviates from the regression line have been removed. Only two of these are starburst candidate galaxies with $W1 - W2 > 0.25$ mag. Magnitude error bars are mostly vanishingly small. The green line is the *hyperfit*. There is a skew distribution around the fit, but this does not seem to be related to unusual redshifts or inclinations.

nitude is `mag_auto_i` and the axial ratio is `b_image_g/a_image_g`. The correlation is strong, as seen in Table 6, where the *hyperfit* χ^2 is shown. The *rms* difference in inclinations between DELVE and Table 3 is 15 degrees, similar to what was found in the previous section, with DELVE delivering a slightly better χ^2 . With 2.5σ deviates rejected, the vertical scatter is 1.27 mag.

Armed with accurate positions from HyperLeda and DELVE, we can perform a match with a catalogue of galaxy magnitudes prepared for the 4MOST collaboration (Taylor et al. 2023) and based on the VISTA Hemisphere Survey.

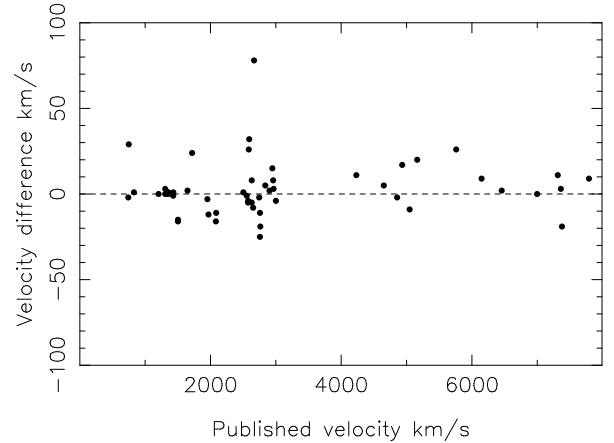


Figure 10. Comparison of WALLABY velocities from Tables 4 and 5 in the NGC 5044 field with published heliocentric velocities.

We present the J-band TFR in Figure 16. The vertical scatter is 1.45 mag. Also available from HyperLeda are I magnitudes from the DENIS survey (Paturel et al. 2005). Figure 17 shows this TFR, and its vertical scatter is 0.81 mag. This catalogue covers the southern hemisphere with cutouts for the Magellanic Clouds and low Galactic latitudes. The χ^2 per degree of freedom for these four TFRs is given in Table 6. The TFR for the DENIS data is well fit by equation (14) of the SFI++ sample of Springob et al. (2018). The magnitude extinction correction ($1.05 \log(a/b)$) of Giovanelli et al. (1994) does not change χ^2 significantly. We provide slopes and zeropoints of the *hyperfits* in Table 8, but note that these quantities will be determined with larger samples in the full WALLABY survey. The χ^2 was calculated with

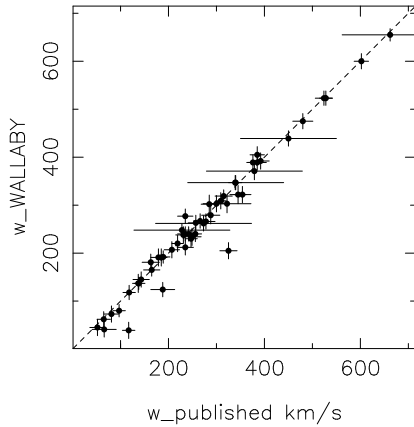


Figure 11. Comparison of WALLABY velocity widths from Tables 4 and 5 in the NGC 5044 field with velocity widths compiled in EDD (Tully et al. 2009). The dashed line is the 1:1 line. **Below:** The difference plot with the 3 most deviant points removed.

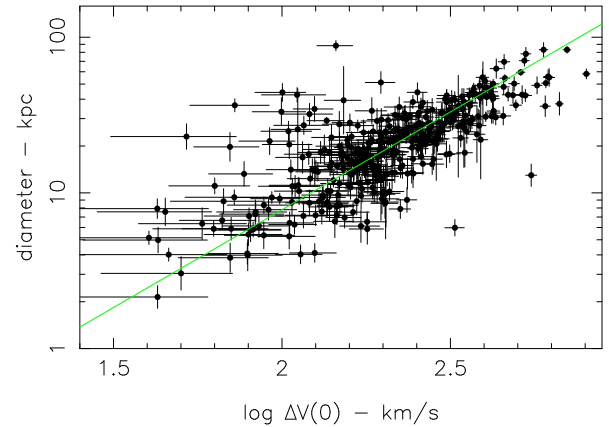
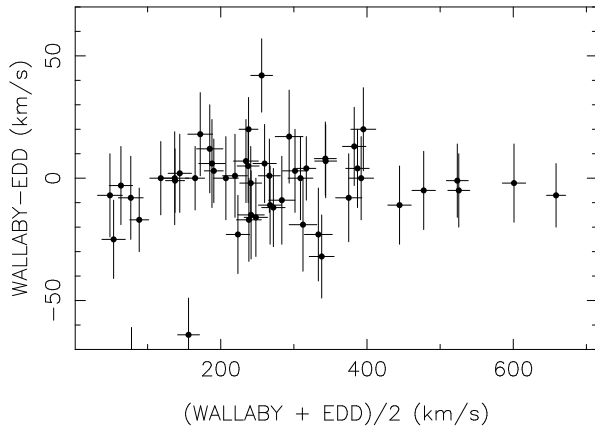


Figure 12. The relation between PGC diameter and inclination corrected velocity width for the NGC5044 field. A Hubble constant of $73 \text{ km s}^{-1} \text{ Mpc}^{-1}$ was adopted. The green line is the *Hyperfit*.

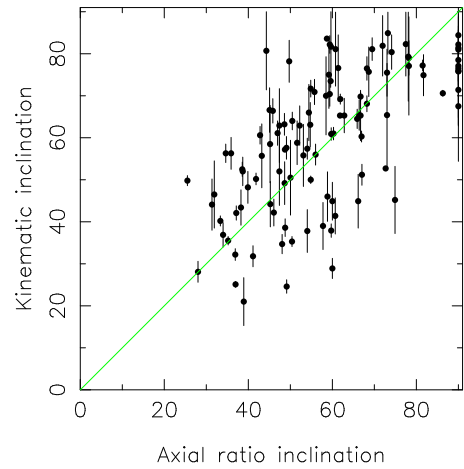


Figure 13. Inclinations from WALLABY kinematic modelling (Deg et al. 2022) and those used here from ellipse fitting. The latter have not had uncertainties measured. The green line is equality.

Table 6. TFR Quality of linear fit, NGC 5044 field

TFR	Source	Figure	S/N cutoff	χ^2	n
<i>i</i> mag	DELVE DR2	15	none	1.48	325
J mag	4MOST	16	3.7	5.34	189
I mag	DENIS	17	3.0	3.30	303
W1 mag	WISE	9	3.7	3.20	344

Linear fits were used, not *hyperfits*.

an intrinsic TFR scatter of 0.40 mag (Masters et al. 2014) and an assumed inclination error of 12.5 degrees (see below). The photometric uncertainties in DELVE and 4MOST are included but are negligible.

4.4 WALLABY detections with no optical counterpart

In Tables 1-3 WALLABY pilot survey galaxies not detectable in WISE or DECaLS and free from close companions are a fraction of a percent of the total. In a sample of 1700 galaxies statistical juxtaposition of noise in the datacubes will occur, and, although all SoFiA detections have been examined, confirmation is needed. Deeper optical imaging and higher resolution HI maps are desirable for these objects. These sources extend over multiple WALLABY beams, so the velocity range is not smeared out. They are being studied intensively in another WALLABY program (O’Beirne et al. 2024), and thus

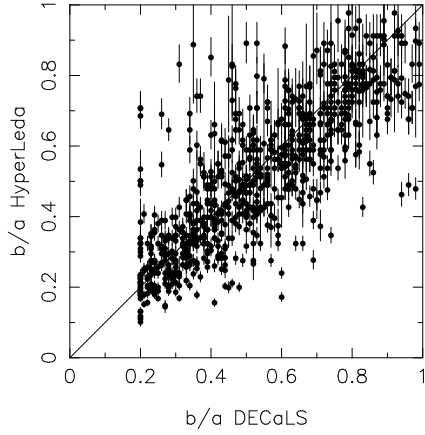


Figure 14. Axial ratios from HyperLeda for PGC galaxies and those used here from ellipse fitting. The line is the 1:1 line.

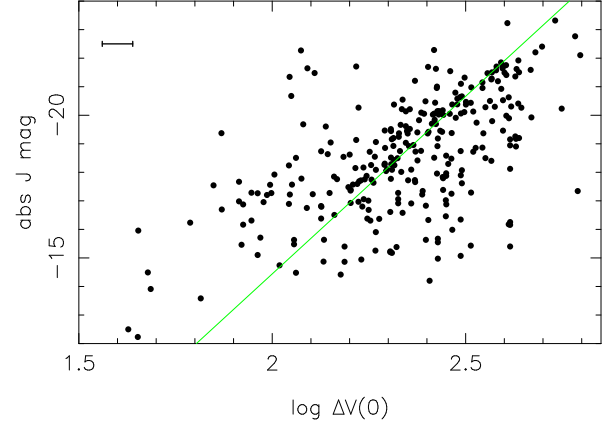


Figure 16. TFR in J magnitudes from 4HS (the 4MOST Hemisphere Survey) for the NGC 5044 field. The error bar shows an average velocity width uncertainty.

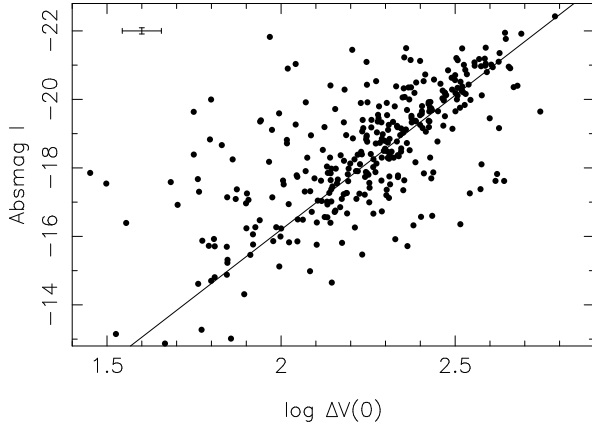


Figure 15. TFR from DELVE DR2 i magnitudes for galaxies with PGC positions in the NGC 5044 field. The error bar is an average velocity width uncertainty and a peculiar velocity uncertainty of 200 km s^{-1} . The line is the TFR of Springob et al. (2018).

we shall not go into detail here. Their relationship to those Ultra Diffuse Galaxies (UDGs; Mancera Pina et al. 2019, 2020), which are not HI rich (For et al. 2023) remains to be explored.

5 DISCUSSION

5.1 Combined fields

We combine the TFRs for the three fields in Figure 18. The intercepts of the three TFRs are not different within the uncertainties. According to the IRSA dust map viewer the Schlafly & Finkbeiner (2011) extinction in Vela varies from

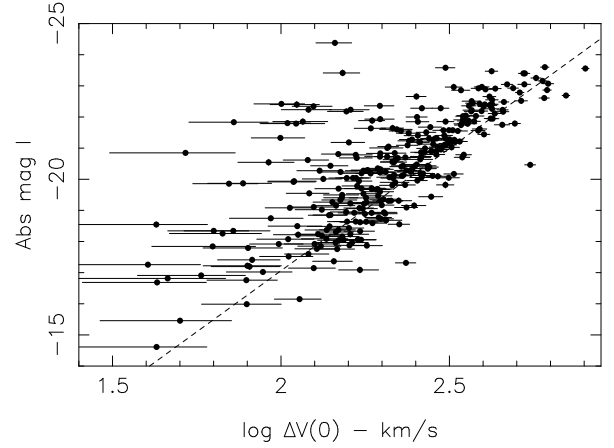


Figure 17. TFR in I magnitudes from the DENIS survey for the NGC 5044 field. The dashed line is from Springob et al. (2018).

$E(B-V) = 0.17 \text{ mag}$ in the NE region of our field to 0.475 mag in the SW. In the W1 bandpass this range is $(0.037, 0.103) \text{ mag}$ in A_{W1} . This is not responsible for the scatter in Figure 7 or Figure 19. The other two fields are high latitude fields with $E(B-V) = 0.03$ and 0.06 mag .

5.2 A simulation

The full WALLABY survey will address the growth of structure in the Universe, measuring $f\sigma_8$ with high statistical accuracy (Said et al. 2020) and discovering large scale flows in the accessible volume. As a simple test we inserted a 500

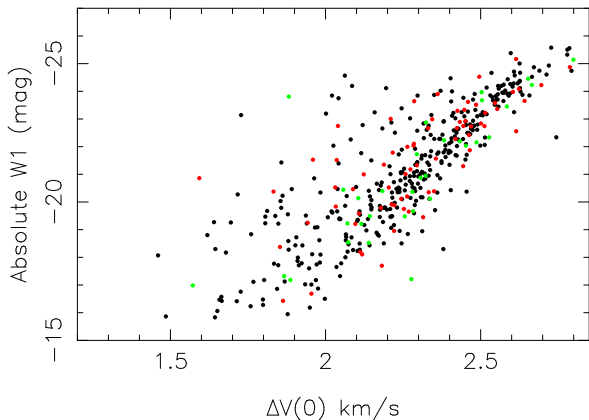


Figure 19. The three WALLABY phase 2 pilot survey TFR relations combined. NGC5044 is in black, Vela is in red and NGC4808 in green.

km s^{-1} bulk flow in a 10^4 Mpc^3 volume of the NGC 5044 field at 5500 km s^{-1} redshift, as depicted in Figure 20. Scatter of 1.04 mag rms from the $(W1, \Delta V(0))$ TFR was added to the Hubble flow and the input flow velocity was recovered with 2.5σ significance from 156 galaxies. This bodes well for the full survey and suggests that expectations based on the simulations of Boubel et al. (2024) with 7341 ALFALFA galaxies will be realised. The average TFR scatter assumed in their error model for these 156 galaxies was 0.93 mag .

The full WALLABY survey will cover regions of high and low extinction, and therefore the W1 magnitudes have a significant advantage for measuring peculiar velocities on large scales. If these measurements can be automated for $\sim 10^5$ galaxies, this approach would be preferred. If not, Table 6 suggests that DELVE DR2 would provide a good alternative, better still if that can be combined with an extinction map to correct the I magnitudes and a higher throughput filter on the DELVE survey than the PGC catalogue to ensure unique matching.

5.3 New positions of the Great Attractor and Vela from the WALLABY addition to CosmicFlows4

Figure 20 shows comparatively a map of the Norma region as seen from the computation of the linear velocity field and corresponding density field, thanks to peculiar velocities (Courtois et al. 2023). The left panel shows the reconstruction with CosmicFlows4 (CF4) galaxies only (black dots) while the right panel shows the reconstruction with the WALLABY pilot data added (coloured dots) to CF4. Before the addition of WALLABY data the Great Attractor was located a bit closer to us at $\text{SGX-SGY} = (-30, 0) \text{ Mpc/h}$. The new location is at $\text{SGX-SGY} = (-40, +10) \text{ Mpc/h}$ (see Tables 7a&b). The signal to noise of the Linear density field reconstruction at the Great Attractor location is a strong 15σ . We also note that the velocity flow around Coma cluster is modified. Now Coma appears as a clearly detached cluster.

This figure corresponds to the Great Attractor position in

the Supergalactic plane SGX-SGY. It is a slice of $\pm 5 \text{ Mpc/h}$ thickness, centred at supergalactic $\text{SGZ} = 0 \text{ Mpc/h}$. The blue and red background colours show the linear density field recovered from the CosmicFlows4 compendium of peculiar velocities (Courtois et al. 2023). The black dots are galaxies from the CosmicFlows4 catalogue. The coloured dots are the WALLABY pilot data. Also the velocity flow around Coma is modified. Now Coma appears as a clearly detached cluster. This figure corresponds to the Vela supercluster position in the Supergalactic plane SGY-SGZ. It is a slice of ± 5 i.e. 10 Mpc/h thickness, centered at supergalactic $\text{SGX} = -130 \text{ Mpc/h}$. The blue and red background colours show the linear density field recovered from the CosmicFlows4 compendium of peculiar velocities (Courtois et al. 2023). The green square is the position of Vela as found by Kraan-Korteweg et al. 2017 from redshift surveys. The red triangle was the position of Vela as found by Courtois et al. 2019 using the V-web of CF3. The black dots are galaxies from the CosmicFlows4 catalogue. The coloured dots are the WALLABY pilot data.

The region scrutinized in Figure 21 is a slice at supergalactic $\text{SGX} = -130 \text{ Mpc/h}$. A clear over-density of galaxies is seen on both sides of the zone obscured by the Milky Way disc (vertical on this figure) at $\text{SGZ} = -130 \text{ Mpc/h}$. This is what was named the "Vela wall" of the "Vela supercluster": a filament running across the ZOA and extending in total to more than $6,000 \text{ km s}^{-1}$ from the redshift surveys' point of view. The black arrows on this figure correspond to the peculiar (gravitational) velocity field. A striking result is that, quite independently, the new WALLABY data confirms the Vela position published by Kraan-Korteweg et al. (2017). The Vela supercluster extends from side to side across the ZOA. Since it is a three-dimensional velocity field, on the figure these vectors are projected onto the plane SGY-SGZ. The red triangle on this Figure 21, was published in 2019 by Courtois et al. as a point of convergence of the V-web located at $\text{SGX-SGY-SGZ} = (-13,000; 7,000; -9,000) \text{ km s}^{-1}$. This location is the central region of a gravitational basin of attraction located on the sky in the Vela constellation direction. This Vela large-scale structure is not part of the larger Shapley attractor as one can see that there is a clear delimitation of the streamlines splitting between these two basins. Consequently, the cross-analysis of redshift surveys data (Kraan-Korteweg 2017) and the new addition of WALLABY data in the southern hemisphere to the peculiar velocity surveys data confirms the position of the Vela supercluster at $\text{SGY-SGZ} = (40; -140) \text{ Mpc/h}$. The signal to noise of the linear density field reconstruction at the Vela location has strong 4σ significance. We also note that before the WALLABY data the cluster NGC5044 was not well reconstructed by CosmicFlows-4 catalogue. Even worse there was an under-density (a cosmic void) reconstructed at its location. The addition of the WALLABY pilot data, causes NGC5044 now to appear on the map at $\text{SGY-SGZ} = (100; 0) \text{ Mpc/h}$.

CosmicFlows4 is the most advanced representation of the flow field of galaxies within $20,000 \text{ km s}^{-1}$, using redshift independent distances. A multiwavelength baryonic TFR has been adopted for this purpose, and in the Appendix we describe the calibration *pro-tem* of our single wavelength (W1) baryonic TFR, so that pilot survey distances can be introduced into the CF4 database, and a new reconstruction run. Reconstruction is the process of calculating the gravitational field of galaxies with known distances, and thus, in the lin-

Table 7. (a) Large scale structure parameters Positions of the Great Attractor (GA) and Vela supercluster in CF4 alone in black and with the addition of WALLABY in bold. The radius of the corresponding spherical overdensity is given in the last column.

Structure	SGX Mpc /h	SGY Mpc /h	SGZ Mpc /h	overdensity at the peak	distance to $\delta=0$ Mpc /h
GA	-49/ -40	4/ 5	8/ 0	0.7/ 0.9	30/ 40
Vela	-130/ / -130	-15/ / 40	-150/ / -140	-0.4/ / 0.5	60/60

Structure	vx km s ⁻¹	vy km s ⁻¹	vz km s ⁻¹	Vbulk km s ⁻¹
Great Attractor	-153/ -102	42/ 78	52/ 37	206/ 188
Vela.	220/ -349	82/ -39	252/ -83	353/ 394

Table 7. (b) Bulk flow velocities computed within sphere of radius 20 Mpc/h centered around GA [-40,5,0] Mpc/h and Vela [-130,40,-140] Mpc/h. The addition of pilot phase 2 WALLABY data modifies the amplitude and direction of the velocity field. The CF4 alone values (in black) and strongly modified when adding WALLABY data (in bold) in the region of Vela supercluster where the bulk flow changes direction towards negative supergalactic X and Z axis and is enlarged by an amount of 50km/s reaching 394 km s⁻¹. This shows that Vela is a main gravitational actor in the southern sky large-scale structures.

Table 8. Summary of data and cuts

Target group	Fields	Area deg ²	PDR2	Table tally	SNR cut	incl cut†	used TFR
N4808	1	30	231	201 T1	3.7	96	29
Vela	1	30	203	143 T2	3	34	71
N5044	4	120	1326	1238 T3	3.7*	26	348
Total	6	180	1760	1582		398	448

*also a 3 σ TFR deviates cut

†Numbers cut for $i > 45^\circ$

Table 9. Hyperfits*

Field	Slope	\pm	β mag	\pm	σ mag	\pm mag
NGC 4808 Fig 3	-10.20	0.76	2.54	1.82	0.65	0.13
Vela Figure 7	-11.57	0.84	5.51	1.99	0.90	0.12
NGC 5044 Fig 9	-10.68	0.30	3.26	0.69	0.94	0.06

* $M(W1) = \alpha \log \Delta V(0) + \beta$. Slope = α ; σ = scatter.

Columns headed \pm are uncertainties in columns to their left.

ear approximation, the peculiar velocity field. At this stage we are not able to include WALLABY selection effects in the reconstruction, as we are still learning what these are. The S/N ratio cutoff of the WALLABY survey is now known (Westmeier et al. 2022; Murugesan et al. 2024), which will allow selection effects to be simulated. The first plot (Figure

20) is a SGX-SGY slice at SGZ=0. The red blob across the Zone Of Avoidance (ZOA) (which is horizontal SGY=0) and SGX=-40 Mpc/h is the Great Attractor. Figure 21 is perpendicular to it. The effect of adding the WALLABY pilot survey galaxies is to greatly increase the spatial resolution of the flow field.

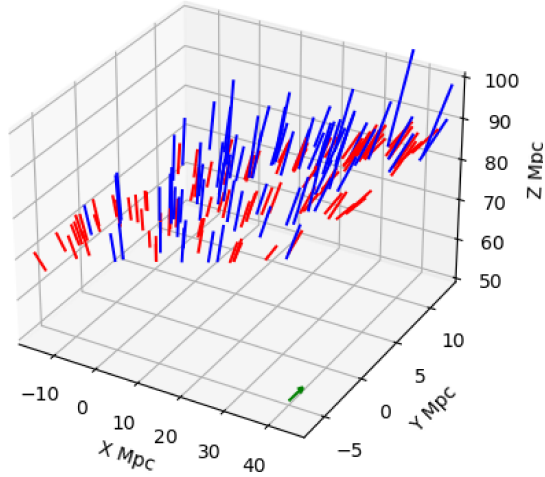


Figure 19. A portion of the NGC 5044 field in real space, where the Z coordinate is in the radial direction, and the tangential coordinates point N (Y) and E (X). The difference between the TFR distance times H_0 and the redshift is the peculiar velocity, shown by the length of the arrows. Red is redshift and blue is approaching. These have been scaled down by a factor of ten for clarity. A bulk flow of 500 km s^{-1} depicted by the barely visible green arrow in the foreground, added to these data can be retrieved, as described in §5.2.

6 CONCLUSIONS

The WALLABY Pilot Survey has taught us a number of things that can be built on in the full survey, which is now under way.

- (1) The TFR is clearly observed in the three fields of the WALLABY Pilot Survey Phase 2 and can be used for redshift independent distances. A summary is given in Table 9. There are ten times the number of galaxies in these fields as there are for these parts of the sky in CosmicFlows4.
- (2) Axial ratios of galaxies from isophotal ellipse fitting in the optical correlate with disk inclinations from WALLABY kinematic modelling and with HyperLeda axial ratios. The scatter in this relation allows our axial ratio uncertainties to be estimated, and this comes close to explaining the TFR scatter we see. Measuring and controlling errors in inclination are crucial to understanding the scatter in the TFR and estimating distances.
- (3) A diameter/velocity-width scaling relation with scatter comparable to the TFR can be readily constructed from HyperLeda diameters. Further work is warranted on investigating the origin of this relation and potentially combining it with the TFR to obtain better distance estimates.
- (4) For WALLABY sources matched to PGC galaxies, 4MOST magnitudes based on the VISTA Hemisphere Survey can be used to make a J magnitude TFR, and DELVE (DENIS) magnitudes can be used to make an *i* (I) magnitude

- TFR. These would require calibrations before they could be used to investigate cosmic flows. By calibrations we mean the slope of the TFR and any nonlinearity. The zeropoint affects Hubble constant determinations, but not peculiar velocities.
- (5) A number of optical non-detections have HI properties similar in hydrogen mass to luminosity ratios seen in one or two extreme objects in the Local Volume HI Survey of Koribalski (2018). These number $\sim 0.3\%$ of the HI detections in the NGC 5044 field. Confirmation of these objects is required.
 - (6) Forecasts for constraints from the full WALLABY survey on the growth rate of structure at the current epoch and for the measurement of large scale flows seem sound based on the pilot survey.
 - (7) Addition of WALLABY galaxies to CosmicFlows4 increases the spatial resolution of the flow field because the higher sampling density affords more detail in the reconstruction.

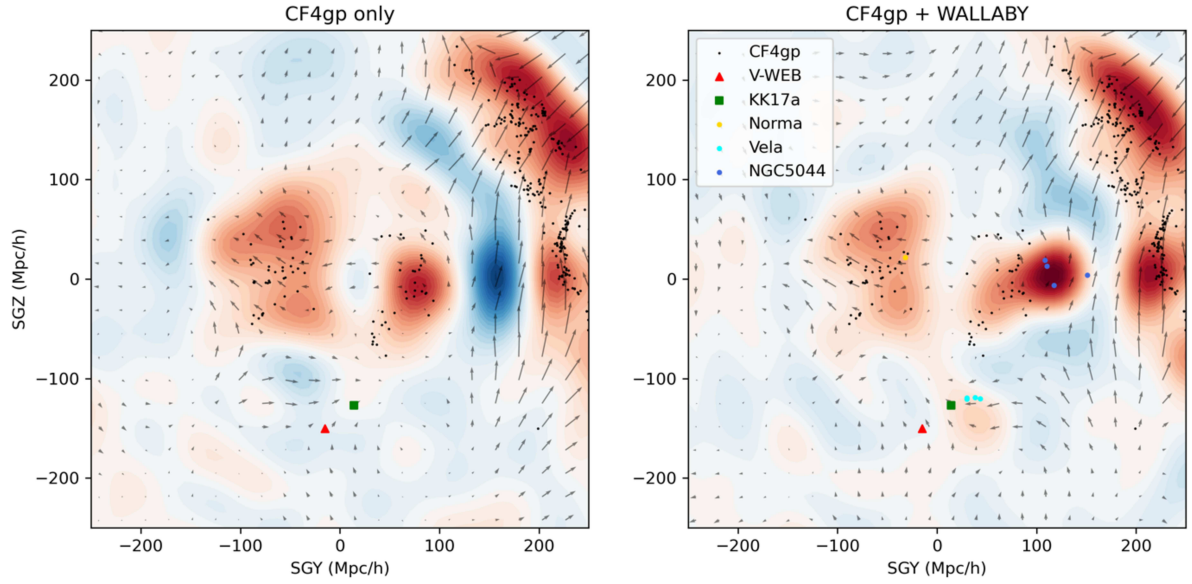


Figure 20. In the left panel is the flow field solution computed with only CF4 data. In the right panel is the solution using distances from CF4 + WALLABY. WALLABY data points are in colour. The background red shading corresponds to mass overdensity and blue to relative underdensity. The arrows show the direction of the consequent flow field.

Figure 21. A SGY-SGZ slice at $SGX = -130$ Mpc/h. Left and right panels are as in the previous figure. The Vela supercluster is near the ZOA (which is at $SGY = 0$ vertical). The position of Vela from Kraan-Korteweg et al. (2017) is a green square. And the position of Vela as a knot of the V-web (Courtois et al. 2019) is a red triangle.

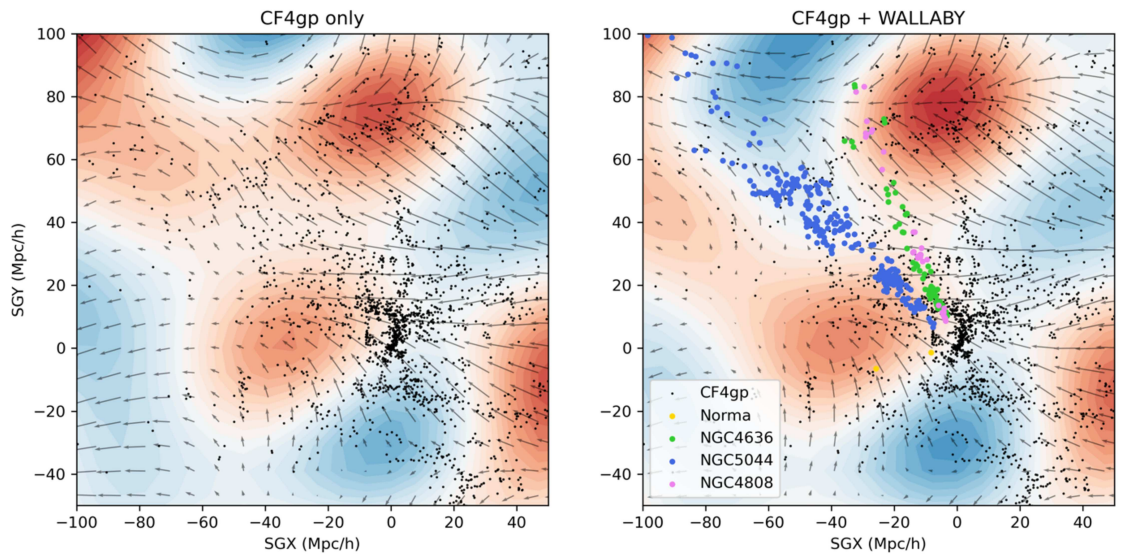


Table 1. WALLABY data and WISE photometry NGC 4808 field

Name	RA	Dec	v_{helio}	b/a	W1	$\delta W1$	W ₅₀	δW_{50}	S/N	alias
(1)	J2000	(3)	km s ⁻¹	(5)	mag	mag	km s ⁻¹	km s ⁻¹	(10)	(11)
WALLABY_J124747+042017	191.94598	4.33818	987	0.878	10.28	0.03	46	18	4.2	NGC 4688
WALLABY_J124805+065910	192.02299	6.98568	13424	0.760	12.83	0.02	130	19	2.1	PGC043228
WALLABY_J124822+082925	192.09509	8.49036	1011	0.666	7.35	0.01	424	19	2.9	NGC 4698
WALLABY_J124911+032310	192.29604	3.38610	722	0.739	9.50	0.01	167	16	6.0	NGC 4701
WALLABY_J124915+043926	192.31544	4.65741	2668	0.860	12.92	0.03	75	17	4.9	UGC 7976
WALLABY_J124923+050820	192.34853	5.13909	12410	0.725	13.83	0.01	212	25	1.8	PGC3395349
WALLABY_J124925+042328	192.35762	4.39118	2643	0.550	13.82	0.04	104	18	3.9	PGC1267592
WALLABY_J124935+033620	192.39824	3.60573	7085	0.897	12.46	0.01	166	18	4.3	PGC043361
WALLABY_J124937+074725	192.40498	7.79054	16420	0.739	14.94	0.02	273	19	2.0	
WALLABY_J124944+044608	192.43346	4.76898	8441	0.370	12.28	0.01	146	19	2.6	PGC043389
WALLABY_J124947+035042	192.44933	3.84521	698	0.440	13.75	0.03	35	17	5.4	UGC 7983
WALLABY_J124950+025100	192.45959	2.85022	1159	0.220	9.82	0.01	208	19	2.2	UGC 7982
WALLABY_J124957+040438	192.49109	4.07742	10202	0.680	13.60	0.02	218	18	4.1	PGC1263188
WALLABY_J124959+054921	192.49675	5.82272	630	0.720	13.80	0.02	109	18	3.3	PGC1289538
WALLABY_J125012+073442	192.55397	7.57855	11451	0.760	10.73	0.01	274	19	3.1	AGC225050
WALLABY_J125103+072753	192.76622	7.46492	15171	0.640	12.37	0.01	297	20	2.0	PGC1322513
WALLABY_J125112+045132	192.80307	4.85892	7532	0.884	10.18	0.01	233	18	3.5	NGC 4734
WALLABY_J125114+052031	192.81215	5.34211	7514	0.977	13.45	0.02	74	17	4.6	AGC225201
WALLABY_J125121+063829	192.84126	6.64150	14998	0.740	14.21	0.02	124	17	5.4	PGC1304685
WALLABY_J125127+054748	192.86482	5.79682	14439	0.710	12.50	0.01	455	19	2.6	PGC1289326
WALLABY_J125133+080241	192.88995	8.04494	3597	0.888	13.49	0.08	130	18	4.0	PGC043556
WALLABY_J125134+055147	192.89421	5.86332	14592	0.674	12.03	0.02	401	24	1.8	PGC1290429
WALLABY_J125156+035954	192.98697	3.99838	7684	0.574	15.41	0.02	206	28	1.7	PGC1261946
WALLABY_J125211+043045	193.04642	4.51261	19307	0.790	13.03	0.01	271	19	2.6	PGC4345126
WALLABY_J125215+042728	193.06422	4.45782	696	0.570	15.42	0.11	57	19	2.5	AGC226122
WALLABY_J125224+071046	193.10010	7.17953	14948	0.325	13.73	0.03	230	17	6.6	PGC1315615
WALLABY_J125233+031517	193.13998	3.25474	14620	0.666	12.38	0.01	295	22	1.9	PGC1248106
WALLABY_J125243+075643	193.17969	7.94529	11588	0.740	13.27	0.02	201	22	1.9	PGC1335032
WALLABY_J125258+073025	193.24283	7.50694	16023	0.790	12.56	0.02	421	19	3.0	PGC043729
WALLABY_J125303+070944	193.26555	7.16228	15196	0.600	16.16	0.06	111	19	2.3	PGC5509705
WALLABY_J125308+081035	193.28596	8.17653	14834	0.490	16.03	0.05	123	41	1.1	PGC434576
WALLABY_J125311+032639	193.29700	3.44418	2789	0.900	16.54	0.20	29	19	2.6	PGC166147
WALLABY_J125313+042746	193.30641	4.46279	725	0.688	10.35	0.01	87	16	6.2	NGC 4765
WALLABY_J125334+060947	193.39287	6.16324	13460	0.410	12.69	0.02	160	19	2.5	
WALLABY_J125339+040434	193.41631	4.07620	887	0.710	14.69	0.04	40	18	3.7	AGC224229
WALLABY_J125340+064728	193.42010	6.79115	7630	0.808	11.88	0.01	206	19	2.2	PGC043817
WALLABY_J125341+034603	193.42392	3.76761	19644	0.851	13.03	0.02	145	19	3.0	PGC1258221
WALLABY_J125343+040920	193.43007	4.15566	772	0.825	14.74	0.05	39	19	2.6	PGC1264260
WALLABY_J125413+052149	193.55656	5.36375	14499	0.544	12.01	0.01	312	19	2.6	PGC4676508
WALLABY_J125419+064115	193.57948	6.68763	3633	0.785	13.64	0.01	92	27	1.7	PGC3091848
WALLABY_J125431+050959	193.63210	5.16657	19563	0.604	12.72	0.01	484	45	1.0	PGC1279102
WALLABY_J125443+050110	193.68056	5.01958	10661	0.533	16.33	0.08	120	18	3.4	
WALLABY_J125443+080310	193.68300	8.05288	2520	0.715	11.23	0.01	243	19	3.1	NGC 4791
WALLABY_J125445+045357	193.69009	4.89937	7453	0.650	15.17	0.06	123	19	2.8	PGC1274939
WALLABY_J125450+072542	193.71011	7.42845	15011	0.617	13.43	0.01	274	25	1.8	PGC1321584
WALLABY_J125500+051140	193.75122	5.19446	19741	0.790	15.73	0.03	79	18	4.5	PGC3480219
WALLABY_J125507+040229	193.78165	4.04148	14467	0.972	12.04	0.01	91	19	2.7	PGC1262572
WALLABY_J125509+075453	193.79150	7.91487	2655	0.551	12.18	0.02	178	18	3.7	UGC 8042
WALLABY_J125515+081543	193.81377	8.26203	21390	0.850	12.30	0.01	169	17	4.9	PGC1343076
WALLABY_J125516+025347	193.81685	2.89662	2803	0.664	9.59	0.01	365	18	3.3	NGC 4799
WALLABY_J125520+050620	193.83734	5.10573	10706	0.548	13.85	0.02	200	21	1.9	PGC3480237
WALLABY_J125548+041805	193.95232	4.30158	760	0.537	8.71	0.02	269	15	7.7	NGC 4808
WALLABY_J125548+045901	193.95166	4.98387	14632	0.525	12.33	0.01	430	18	4.3	PGC1276334
WALLABY_J125549+040049	193.95634	4.01383	712	0.518	12.24	0.03	124	17	5.5	UGC 8053
WALLABY_J125556+075542	193.98351	7.92859	12464	0.495	12.68	0.01	299	34	1.4	PGC4538018
WALLABY_J125603+045202	194.01451	4.86747	1375	0.800	14.06	0.05	42	17	4.5	PGC5057592

continued in full in MNRAS

Table 2. WALLABY data and WISE photometry Vela field

Name	RA	Dec	v_{helio}	b/a	W1	$\delta W1$	W ₅₀	δW_{50}	S/N	alias
(1)	J2000	(3)	km s ⁻¹	(5)	mag	mag	km s ⁻¹	km s ⁻¹	(10)	(11)
WALLABY_J094317-452105	145.82089	-45.35157	5340	0.313	14.04	0.13	229	17	5.7	
WALLABY_J094325-453019	145.85829	-45.50539	12065	0.616	13.72	0.05	251	18	3.7	
WALLABY_J094333-452200	145.89011	-45.36670	18231	0.511	11.49	0.02	143	19	2.6	PGC527583
WALLABY_J094429-464515	146.12170	-46.75434	17251	0.499	13.55	0.05	277	19	2.3	
WALLABY_J094524-480828	146.35260	-48.14116	880	0.200	14.56	0.09	75	15	8.0	
WALLABY_J094533-462130	146.39050	-46.35859	7502	0.430	15.30	0.07	114	18	3.4	PGC515934
WALLABY_J094613-471709	146.55690	-47.28599	14082	0.500	12.57	0.05	217	18	4.3	
WALLABY_J094622-463856	146.59392	-46.64899	2704	0.300	11.18	0.02	291	16	6.7	
WALLABY_J094723-431306	146.84944	-43.21851	5318	0.479	12.93	0.03	154	32	1.7	
WALLABY_J094814-464424	147.05835	-46.74026	17507	0.422	14.26	0.02	218	17	5.7	
WALLABY_J094819-442224	147.08121	-44.37339	18139	0.281	12.27	0.01	272	35	2.0	PGC538024
WALLABY_J094828-472216	147.11841	-47.37133	17106	0.470	12.35	0.01	297	19	2.5	PGC502430
WALLABY_J094830-464320	147.12833	-46.72243	17352	0.548	14.02	0.04	249	17	4.5	PGC511516
WALLABY_J094840-452959	147.16727	-45.49980	13467	0.226	13.01	0.02	376	19	3.1	
WALLABY_J094854-462741	147.22504	-46.46154	17222	0.536	13.28	0.02	279	19	3.2	
WALLABY_J094855-435404	147.23100	-43.90133	19445	0.873	13.13	0.02	350	17	4.6	PGC543149
WALLABY_J094924-454230	147.35231	-45.70839	5284	0.378	12.88	0.03	98	18	4.5	
WALLABY_J094926-435730	147.36195	-43.95849	19448	0.859	13.61	0.02	203	18	4.0	
WALLABY_J094940-454322	147.41983	-45.72292	16372	0.290	11.68	0.01	458	19	2.3	PGC096455
WALLABY_J094959-481705	147.49632	-48.28491	5212	0.220	12.10	0.03	270	16	6.1	PGC489114
WALLABY_J095019-452605	147.57959	-45.43482	12136	0.506	11.70	0.01	192	19	2.2	PGC309881
WALLABY_J095019-441017	147.58247	-44.17142	19387	0.864	12.99	0.02	120	19	2.5	PGC309880
WALLABY_J095031-461322	147.63036	-46.22299	13532	0.385	16.03	0.06	220	18	4.5	PGC517483
WALLABY_J095053-432902	147.72421	-43.48414	2699	0.717	14.04	0.05	151	31	3.8	PGC548188
WALLABY_J095101-451536	147.75775	-45.26022	11295	0.274	14.65	0.05	161	18	4.5	PGC528651
WALLABY_J095126-452831	147.85852	-45.47532	12124	0.341	13.48	0.02	269	17	5.0	PGC526385
WALLABY_J095131-440121	147.88051	-44.02256	13106	0.415	12.22	0.01	477	19	2.5	PGC028395
WALLABY_J095159-443357	147.99901	-44.56604	19297	1.000	15.02	0.03	101	19	2.2	
WALLABY_J095205-443809	148.02348	-44.63591	18041	0.536	12.68	0.01	254	32	1.5	PGC535167
WALLABY_J095211-464251	148.04860	-46.71441	13589	0.321	13.47	0.02	294	17	4.8	PGC511580
WALLABY_J095234-475517	148.14436	-47.92139	17230	0.738	13.98	0.03	150	15	7.3	
WALLABY_J095239-470647	148.16661	-47.11310	1820	0.900	13.03	0.07	73	19	2.0	PGC506395
WALLABY_J095244-474722	148.18340	-47.78953	5390	0.390	13.92	0.10	115	18	3.6	PGC495718
WALLABY_J095311-451624	148.29988	-45.27333	11263	0.762	13.69	0.04	206	19	3.1	PGC528542
WALLABY_J095316-431054	148.31738	-43.18174	18933	0.600	14.28	0.02	89	22	1.9	
WALLABY_J095347-455759	148.44792	-45.96661	7089	0.200	11.14	0.01	367	19	2.4	PGC028528
WALLABY_J095354-433845	148.47746	-43.64592	7727	0.432	14.19	0.03	175	17	4.8	
WALLABY_J095423-443318	148.59874	-44.55511	10029	0.853	13.65	0.04	150	18	3.5	PGC536076
WALLABY_J095433-440456	148.63873	-44.08222	17770	0.948	13.77	0.02	270	19	2.8	
WALLABY_J095441-440640	148.67125	-44.11118	17882	0.483	12.71	0.02	252	19	2.3	PGC540776
WALLABY_J095448-462159	148.70078	-46.36654	7074	0.824	12.91	0.02	186	17	5.0	PGC515876
WALLABY_J095449-461903	148.70421	-46.31764	16160	0.721	14.67	0.04	275	19	2.4	PGC516415
WALLABY_J095457-480416	148.73886	-48.07116	11541	0.561	11.82	0.02	440	18	3.5	PGC308536
WALLABY_J095532-443931	148.88661	-44.65867	18673	0.799	11.88	0.01	336	18	3.5	PGC534960
WALLABY_J095552-455731	148.96976	-45.95863	12425	0.781	14.85	0.04	93	18	4.0	
WALLABY_J095558-472929	148.99477	-47.49157	19141	0.933	14.40	0.02	120	15	7.9	
WALLABY_J095635-453219	149.14613	-45.53882	13794	0.531	14.43	0.03	174	18	3.8	
WALLABY_J095648-450253	149.20219	-45.04817	19190	0.438	15.53	0.04	228	19	2.3	
WALLABY_J095710-485624	149.29468	-48.94017	3727	0.250	12.83	0.04	40	16	6.5	PGC580713
WALLABY_J095719-465024	149.32941	-46.84004	13024	0.617	13.56	0.02	277	19	3.1	
WALLABY_J095802-444730	149.51060	-44.79173	23768	0.729	14.67	0.02	244	36	3.7	PGC533495
WALLABY_J095809-472057	149.54031	-47.34937	3644	0.896	14.38	0.05	124	17	5.6	
WALLABY_J095813-430817	149.55484	-43.13825	7307	0.396	14.88	0.06	184	18	3.9	
WALLABY_J095824-433328	149.60017	-43.55786	18236	0.608	12.85	0.01	130	19	2.1	PGC547363
WALLABY_J095836-470454	149.65350	-47.08191	3628	0.412	10.89	0.01	109	19	3.2	
WALLABY_J095848-455156	149.70287	-45.86573	3664	0.598	12.09	0.01	196	18	4.0	

Continued in full in MNRAS

ACKNOWLEDGEMENTS

The Australian SKA Pathfinder is part of the Australia Telescope National Facility (<https://ror.org/05qajvd42>) which is managed by CSIRO. Operation of ASKAP is funded by the Australian Government with support from the National Collaborative Research Infrastructure Strategy. ASKAP uses the resources of the Pawsey Supercomputing Centre. Establishment of ASKAP, the Murchison Radio-astronomy Observatory and the Pawsey Supercomputing Centre are initiatives of the Australian Government, with support from the Government of Western Australia and the Science and Industry Endowment Fund. We acknowledge the Wajarri Yamatji as the traditional owners of the Observatory site. WALLABY acknowledges technical support from the Australian SKA Regional Centre (AusSRC) and Astronomy Data And Computing Services (ADACS). AD is supported by a KIAS Individual Grant PG 087201 at the Korea Institute for Advanced Studies. AB acknowledges support from the Centre National d'Etudes Spatiales (CNES), France. PEMP acknowledges support from the Dutch Research Council (NWO) through the Veni grant VI.Veni.222.364. This research was supported partially by the Australian Government through the Australian Research Council Centre of Excellence for Dark Matter Particle Physics (CDM, CE200100008).

This publication makes use of data products from the Wide-field Infrared Survey Explorer, which is a joint project of the University of California Los Angeles, and the Jet Propulsion Laboratory/California Institute of Technology, funded by the National Aeronautics and Space Administration. This research uses services and data provided by the Astro Data Lab at NSF's National Optical-Infrared Astronomy Research Laboratory. The Legacy Surveys consist of three individual and complementary projects: the Dark Energy Camera Legacy Survey (DECaLS; Proposal ID #2014B-0404; PIs: David Schlegel and Arjun Dey), the Beijing-Arizona Sky Survey (BASS; NOAO Prop. ID #2015A-0801; PIs: Zhou Xu and Xiaohui Fan), and the Mayall z-band Legacy Survey (MzLS; Prop. ID #2016A-0453; PI: Arjun Dey). DECaLS, BASS and MzLS together include data obtained, respectively, at the Blanco telescope, Cerro Tololo Inter-American Observatory, NSF's NOIRLab; the Bok telescope, Steward Observatory, University of Arizona; and the Mayall telescope, Kitt Peak National Observatory, NOIRLab. Pipeline processing and analyses of the data were supported by NOIRLab and the Lawrence Berkeley National Laboratory (LBNL). The Legacy Surveys project is honored to be permitted to conduct astronomical research on Iolkam Du'ag (Kitt Peak), a mountain with particular significance to the Tohono O'odham Nation.

NOIRLab is operated by the Association of Universities for Research in Astronomy (AURA) under a cooperative agreement with the National Science Foundation. LBNL is managed by the Regents of the University of California under contract to the U.S. Department of Energy.

This project used data obtained with the Dark Energy Camera (DECam), which was constructed by the Dark Energy Survey (DES) collaboration. Funding for the DES Projects has been provided by the U.S. Department of Energy, the U.S. National Science Foundation, the Ministry of Science and Education of Spain, the Science and Technology Facilities Council of the United Kingdom, the Higher Education Funding Council for England, the National Center

for Supercomputing Applications at the University of Illinois at Urbana-Champaign, the Kavli Institute of Cosmological Physics at the University of Chicago, Center for Cosmology and Astro-Particle Physics at the Ohio State University, the Mitchell Institute for Fundamental Physics and Astronomy at Texas A&M University, Financiadora de Estudos e Projetos, Fundacao Carlos Chagas Filho de Amparo, Financiadora de Estudos e Projetos, Fundacao Carlos Chagas Filho de Amparo a Pesquisa do Estado do Rio de Janeiro, Conselho Nacional de Desenvolvimento Cientifico e Tecnologico and the Ministerio da Ciencia, Tecnologia e Inovacao, the Deutsche Forschungsgemeinschaft and the Collaborating Institutions in the Dark Energy Survey. The Collaborating Institutions are Argonne National Laboratory, the University of California at Santa Cruz, the University of Cambridge, Centro de Investigaciones Energeticas, Medioambientales y Tecnologicas-Madrid, the University of Chicago, University College London, the DES-Brazil Consortium, the University of Edinburgh, the Eidgenossische Technische Hochschule (ETH) Zurich, Fermi National Accelerator Laboratory, the University of Illinois at Urbana-Champaign, the Institut de Ciencies de l'Espai (IEEC/CSIC), the Institut de Fisica d'Altes Energies, Lawrence Berkeley National Laboratory, the Ludwig Maximilians Universitat Munchen and the associated Excellence Cluster Universe, the University of Michigan, NSF's NOIRLab, the University of Nottingham, the Ohio State University, the University of Pennsylvania, the University of Portsmouth, SLAC National Accelerator Laboratory, Stanford University, the University of Sussex, and Texas A&M University.

BASS is a key project of the Telescope Access Program (TAP), which has been funded by the National Astronomical Observatories of China, the Chinese Academy of Sciences (the Strategic Priority Research Program The Emergence of Cosmological Structures Grant # XDB09000000), and the Special Fund for Astronomy from the Ministry of Finance. The BASS is also supported by the External Cooperation Program of Chinese Academy of Sciences (Grant # 114A11KYSB20160057), and Chinese National Natural Science Foundation (Grant # 12120101003, # 11433005). We acknowledge the use of the HyperLeda database (<http://leda.univ-lyon1.fr> and the Siena Galaxy Atlas. That was made possible by funding support from the U.S. Department of Energy, Office of Science, Office of High Energy Physocs under award number DE-SC0020086 and from the National Science Foundation under grant AST-1616414.

We thank WALLABY team member Matthew Colless for reading drafts of this paper and Tobias Westmeier for his management of the WALLABY project. We thank the referee for pointing out some things that needed clarifying.

DATA AVAILABILITY

When released, 21 cm profiles in this paper will be curated by the CSIRO ASKAP Science Data Archive. These profiles can be viewed at <https://github.com/jrmould/wallaby-HI-profiles>.

Table 3. WALLABY data and WISE photometry NGC 5044 field

Name	RA J2000	Dec	v_{helio} km s ⁻¹	b/a	W1 mag	$\delta W1$ mag	W ₅₀ km s ⁻¹	δW_{50} km s ⁻¹	S/N	alias
(1)	(2)	(3)	(4)	(5)	(6)	(7)	(8)	(9)	(10)	(11)
WALLABY_J125700-171910	194.25180	-17.31950	3972	0.620	11.65	0.01	220	19	2.6	PGC044234
WALLABY_J125706-182159	194.27628	-18.36646	16185	0.706	11.29	0.01	88	29	1.6	ESO575-036
WALLABY_J125757-130339	194.48877	-13.06087	5022	0.556	9.53	0.01	215	19	2.8	NGC4838
WALLABY_J125834-164819	194.64464	-16.80551	3843	0.386	13.61	0.01	147	19	3.1	PGC044478
WALLABY_J125836-161333	194.65154	-16.22606	5266	0.000	12.41	0.01	131	19	2.7	
WALLABY_J125843-170913	194.67995	-17.15386	8361	0.485	12.88	0.01	318	19	2.6	PGC044499
WALLABY_J125848-114647	194.70290	-11.77985	4849	0.200	13.61	0.02	154	19	2.2	PGC104987
WALLABY_J125850-145324	194.71039	-14.89014	4874	0.330	14.38	0.02	144	18	4.1	PGC918593
WALLABY_J125855-142319	194.73131	-14.38869	19381	0.000	19.04	0.46	148	18	3.4	
WALLABY_J125859-135141	194.74915	-13.86140	4883	0.496	15.01	0.02	55	19	2.1	PGC932206
WALLABY_J125907-121329	194.77928	-12.22482	1312	0.430	13.37	0.03	80	16	6.0	PGC044549
WALLABY_J125910-161749	194.79179	-16.29707	12931	0.686	13.15	0.02	180	19	3.0	PGC899955
WALLABY_J125912-182326	194.80096	-18.39075	15297	0.000	14.13	0.01	89	19	2.1	PGC868681
WALLABY_J125912-124101	194.80396	-12.68385	3875	0.389	14.65	0.03	134	17	4.5	PGC949183
WALLABY_J125923-120455	194.84590	-12.08215	6349	0.460	12.24	0.01	191	18	4.5	PGC3082105
WALLABY_J125930-135159	194.87573	-13.86649	13996	0.000	13.58	0.01	97	18	3.4	PGC932150
WALLABY_J125930-180055	194.87677	-18.01554	4959	0.430	15.59	0.06	120	17	4.6	PGC873976
WALLABY_J125930-120652	194.87744	-12.11468	6387	0.960	12.91	0.01	129	17	4.7	PGC957468
WALLABY_J125931-140755	194.87987	-14.13200	6451	0.759	11.50	0.01	145	17	4.9	NGC4862
WALLABY_J125932-182203	194.88594	-18.36763	15110	0.603	13.85	0.02	119	17	4.9	
WALLABY_J125932-151419	194.88669	-15.23881	1418	0.571	12.78	0.01	95	19	2.1	PGC3082108
WALLABY_J125939-145813	194.91435	-14.97029	4953	0.221	10.80	0.01	360	17	5.2	PGC044645
WALLABY_J125940-151600	194.91905	-15.26692	4860	0.914	13.54	0.01	97	19	2.7	PGC913440
WALLABY_J125942-140140	194.92767	-14.02790	4368	0.466	10.64	0.01	462	18	3.6	NGC4863
WALLABY_J125942-164952	194.92847	-16.83133	1368	0.450	15.81	0.07	43	18	4.2	
WALLABY_J125943-150804	194.93118	-15.13447	13409	0.945	15.41	0.05	86	19	2.5	PGC915253
WALLABY_J125945-145159	194.93814	-14.86639	2659	0.398	13.20	0.01	147	19	2.7	PGC918920
WALLABY_J125949-200826	194.95747	-20.14056	13972	0.000	14.17	0.02	52	29	1.6	
WALLABY_J125951-150446	194.96494	-15.07954	12208	0.676	13.05	0.02	271	18	3.4	PGC916026
WALLABY_J125956-192430	194.98334	-19.40843	826	0.360	14.48	0.03	45	16	6.7	PGC044681
WALLABY_J125959-143124	194.99905	-14.52352	2576	0.247	13.79	0.01	67	17	4.7	PGC923490
WALLABY_J130004-154055	195.01862	-15.68214	1135	0.200	14.47	0.05	121	18	3.3	PGC907834
WALLABY_J130004-152151	195.02060	-15.36439	1589	0.200	10.74	0.01	117	18	4.3	PGC044701
WALLABY_J130010-130042	195.04393	-13.01183	4735	0.201	11.64	0.01	166	19	2.6	PGC044718
WALLABY_J130016-170140	195.06892	-17.02799	4908	0.416	11.14	0.01	240	19	3.0	PGC170439
WALLABY_J130017-122041	195.07176	-12.34494	1581	0.596	11.20	0.01	168	16	6.1	PGC044735
WALLABY_J130018-115758	195.07573	-11.96620	15261	0.978	11.69	0.01	181	18	3.3	PGC959514
WALLABY_J130026-151708	195.10945	-15.28555	4920	0.345	8.74	0.01	600	17	4.9	NGC4877
WALLABY_J130029-181400	195.12294	-18.23359	14628	0.810	15.99	0.05	98	19	2.1	
WALLABY_J130029-133942	195.12305	-13.66192	6392	0.310	16.35	0.07	76	40	1.2	
WALLABY_J130029-133839	195.12349	-13.64420	4331	0.265	12.62	0.01	158	19	3.0	PGC044776
WALLABY_J130032-123039	195.13338	-12.51109	6359	0.680	14.34	0.01	136	17	5.3	PGC951730
WALLABY_J130033-122307	195.14067	-12.38545	2500	0.750	16.43	0.13	45	16	5.8	PGC953585
WALLABY_J130037-143948	195.15587	-14.66346	2701	0.562	10.61	0.01	150	17	5.5	NGC4887
WALLABY_J130043-185429	195.18138	-18.90821	10404	0.498	14.43	0.03	225	17	5.1	PGC862238
WALLABY_J130043-154253	195.18234	-15.71495	1383	0.000	11.74	0.02	85	17	4.9	PGC044812
WALLABY_J130044-142906	195.18745	-14.48505	6422	0.200	14.48	0.03	181	17	5.1	PGC924035
WALLABY_J130047-130944	195.19746	-13.16238	18291	0.631	13.71	0.01	264	18	4.1	PGC941853
WALLABY_J130047-141534	195.19971	-14.25961	4596	0.880	15.48	0.05	117	17	4.8	
WALLABY_J130049-143608	195.20488	-14.60221	6500	0.550	11.60	0.01	259	18	4.3	PGC3098292
WALLABY_J130049-170522	195.20738	-17.08964	4826	0.485	16.45	0.03	101	19	2.3	
WALLABY_J130052-164149	195.21719	-16.69698	4286	0.919	15.21	0.04	79	19	2.9	
WALLABY_J130052-145506	195.21899	-14.91849	13859	0.200	14.99	0.04	78	19	3.1	
WALLABY_J130053-132655	195.22302	-13.44861	2551	0.531	9.37	0.01	230	16	6.1	NGC4897
WALLABY_J130056-135640	195.23347	-13.94450	2654	0.677	9.25	0.01	277	16	6.2	NGC4899
WALLABY_J130057-172247	195.23891	-17.37990	4889	0.731	14.74	0.03	87	18	3.3	PGC884267

Continued in full in MNRAS

Table 4. N5044-DR3 galaxies with 2 published spectra

WALLABY	PGC no	Name	AGC/HIPASS no	V _{sys} km s ⁻¹	Width km s ⁻¹	err km s ⁻¹	S/N	flux Jy km s ⁻¹	V _{wal} km s ⁻¹	W _{wal} km s ⁻¹
J130943-163617	45650	PGC045650	HIPASSJ1309-16	2575	340		5.4	27.18	2574	347
J130943-163617	45650	PGC045650	HIPASSJ1309-16	2576	339	14	8.9	7.62	2574	347
J131234-173225	45877	PGC045877	AGC530053 shg05	2756	385	19	2.2	12.68	2757	389
J131234-173225	45877	PGC045877	HIPASSJ1312-17	2762	376	13	10.0	2.48	2757	389
J132019-123420	46535	NGC5088	HIPASSJ1320-12	1430	235	16	6.6	39.67	1431	240
J132019-123420	46535	NGC5088	AGC530112 shg05	1432	242	13	14.1	42.77	1431	240
J132043-220256	46574	ESO576-040	AGC029511 shg05	2087	185	12	11.6	16.20	2089	191
J132043-220256	46574	ESO576-040	HIPASSJ1320-22	2082	179	16	5.8	3.75	2089	191
J132947-175747	47394	NGC5170	AGC029724	1503	524	18	3.9	71.37	1503	523
J132947-175747	47394	NGC5170	HIPASSJ1329-17	1502	528	13	11.8	5.95	1503	523
J133541-240428	47948	ESO509-074	AGC029872 shg05	2592	354	18	4.1	2.45	2572	322
J133541-240428	47948	ESO509-074	HIPASSJ1335-24	2586	345	17	4.9	8.66	2572	322
J133802-175254	48171	NGC5247	AGC029924 shg05	1356	137	8	53.5	57.73	1354	137
J133802-175254	48171	NGC5247	HIPASSJ1338-17	1355	138	13	32.9	56.62	1354	137

REFERENCES

- Aaronson, M., Huchra, J. & Mould, J. 1979, *ApJ*, 229, 1
- Adams C. & Blake, C. 2017, *MNRAS*, 471, 839
- Bell, R., Said, K., Davis, T. & Jarrett, T. 2023, *MNRAS*, 519, 102
- Bertin, E. & Arnouts, S. 1999, *A&AS*, 117, 393
- Boubel, P., Colless, M., Said, K. & Staveley-Smith, L. 2024, *MNRAS*, 531, 84
- Cluver, M. et al. 2014, *ApJ*, 782, 90
- Cluver, M., Jarrett, T., Dale, D., Smith, J., August, T. & Brown, M. 2017, *ApJ*, 850, 68
- Courtois, H. & Tully, R.B. 2015, *MNRAS*, 447, 1531
- Courtois, H., Tully, R.B., Fisher, J.R., Bonhomme, N., Zavadny, M. & Barnes, A. 2009, *AJ*, 138, 1938
- Courtois, H. et al. 2023, *MNRAS*, 519, 4589
- Courtois, H., Dupuy, A., Guinet, D., Baulieu, G., Ruppin, F., & Brenas, P. 2023, *A&A*, 670, 15
- Deg, N. et al. 2022, *PASA*, 39, 59
- de Vaucouleurs, G., de Vaucouleurs, A., & Corwin, H. 1976, *Second Reference Catalogue of Bright Galaxies*, Univ. Texas Press, Austin
- Djorgovski, S. & Davis, M. 1987, *ApJ*, 313, 59
- Drlica-Wagner, A. et al. 2022, *ApJS*, 261, 38
- Dupuy, A., Courtois, H. & Kubik, B. 2019, *MNRAS*, 486, 440
- For, B.-Q. et al. 2023, *MNRAS*, 526, 3130
- Fu, H. 2024, *arxiv* 2401.13748
- Giovanelli, R., Haynes, M., Salzer, J., Wegner, G., da Costa, L. & Freudling, W. 1994, *AJ*, 107, 2036
- Haynes, M. et al. 2018, *ApJ*, 861, 49
- Hotan, A. et al. 2021, *PASA*, 38, 9
- Jarrett, T., Cluver, M., Taylor, E.N., Bellstedt, S., Robotham, A. & Yao, H. 2023, *ApJ* 946, 95
- Koribalski, B. et al. 2004, *AJ*, 128, 16
- Koribalski, B. et al. 2020, *ApSS*, 365, 118
- Koribalski, B. et al. 2018 *MNRAS*, 478, 1611
- Kourkchi, E., Tully, R.B., Courtois, H., Dupuy, A. & Guinet, D. 2022, *MNRAS*, 511, 6160
- Kowal, C. 1968, *AJ*, 73, 1021
- Kraan-Korteweg, R. et al. 2017, *MNRAS*, 466, L29
- Leisman, L. et al. 2017, *ApJ*, 842, 133
- Lelli, F., McGaugh, S., Schombert, J., Desmond, H. & Katz, H. 2019, *MNRAS*, 484, 3267
- Lineweaver, C., Tenorio, L., Smoot, G., Keegstra, P., Banday, A. & Lubin, P. 1996, *ApJ*, 470, 38
- McGaugh, S., Schombert, J., Bothun, G. & de Blok, W. 2000, *ApJ*, 533, 99
- McGaugh, S. et al. 2021, *AJ*, 162, 202
- Makarov, D., Prugniel, P., Terekhova, N., Courtois, H. & Vauglin, I. 2014, *A&A*, 530, 17
- Mancera Pina, P. et al. 2023, *ApJL*, 833, L33
- Mancera Pina, P. et al. 2020, *MNRAS*, 495, 3636
- Masters, K., Springob, C. & Huchra, J. 2014, *AJ*, 147, 124
- Moustakas, J. et al. 2023, *ApJS*, 269, 3
- Murugesan, C. et al. 2024, submitted to *PASA*
- O’Beirne, T. et al. 2024, in preparation
- Paturel, G., Bottinelli, L. & Gougenheim, L. 1993, *Bulletin d’Information du Centre de Donnée Stellaires*, 42, 33
- Paturel, G. et al. 2003, *A&A*, 412, 45
- Paturel, G. et al. 2005, *A&A*, 430, 751
- Rajohnson, S. et al. 2024, *MNRAS*, in press
- Riess, A. et al. 2022, *ApJ*, 934, 7
- Robotham, A. & Obreschkow, D. 2015, *PASA*, 32, 33
- Said, K., Colless, M., Magoulas, C., Lucey, J., & Hudson, M., 2022, *MNRAS*, 497, 1275
- Schlafly, E. & Finkbeiner, D. 2011, *ApJ*, 737, 103
- Serra, P. et al. 2015, *MNRAS*, 448, 1922
- Springob, C. et al. 2009 *ApJS*, 182, 474
- Springob, C. et al. 2005, *ApJS*, 160, 149
- Taylor, E.N. et al. 2023, *The Messenger*, 190, 46
- Theureau, G., Hanski, M. O., Coudreau, N., Hallet, N. and Martin, J. -M., 2007 *A&A*, 465, 71
- Tully, R.B., Rizzi, L., Shaya, E., Courtois, H., Makarov, D. & Jacobs, B. 2009 *AJ*, 138, 323
- Tully, R.B. & Fisher, J.R. 1977, *A&A*, 54, 661
- Tully, R.B., Courtois, H., Hoffman, Y., & Pomaredo, D. 2014, *Nature*, 513, 71
- Tully, R.B. & Fouqué, P. 1985, *ApJS*, 58, 67
- Wen, X.-Q. et al. 2013, *MNRAS*, 433, 2946
- Westmeier, T. et al. 2021, *MNRAS*, 506, 3962
- Westmeier, T. et al. 2022, *PASA*, 39, 58
- Wright, E. et al. 2010, *AJ*, 140, 1868

Table 5. N5044-DR3 galaxies with 1 published spectrum

WALLABY	PGC no	Name	AGC/HIPASS no	V_{sys} km s^{-1}	Width km s^{-1}	err km s^{-1}	S/N	flux Jy km s^{-1}	V_{wal} km s^{-1}	W_{wal} km s^{-1}
J125907-121329	44549	PGC044549	HIPASSJ1259-12	1308	97	13	11.0	14.13	1312	80
J125931-140755	44610	NGC4862	AGC520377 shg05	6456	143	17	4.7	3.84	6451	145
J125956-192430	44681	PGC044681	HIPASSJ1259-19	829	52	16	6.3	5.03	826	45
J130026-151708	44761	NGC4877	HIPASSJ1300-15	4933	602	15	7.4	16.39	4920	600
J130053-132655	44829	NGC4897	HIPASSJ1300-13	2555	247	13	12.7	29.33	2551	230
J130056-135640	44841	NGC4899	HIPASSJ1301-13B	2653	273	100	34.7	21.09	2654	277
J130059-143042	44847	NGC4902	HIPASSJ1300-14	2631	256	13	12.5	27.93	2624	240
J130107-133053	936912	PGC936912	HIPASSJ1300-13B	1308	65	14	8.7	7.15	1306	62
J130213-145817	44977	NGC4924	HIPASSJ1302-14A	4856	266	14	9.3	8.36	4864	267
J130213-171416	44982	PGC044982	HIPASSJ1302-17	750	117	13	11.5	27.24	726	39
J130225-174046	45006	PGC045006	AGC520412 shg05	4652	480	21	5.7	11.18	4649	475
J130311-172230	45073	PGC045073	HIPASSJ1303-17A	2965	66	25	7.7	10.69	2963	41
J130314-172514	45084	PGC045084	HIPASSJ1303-17B	742	118	13	63.1	93.27	741	118
J130815-210002	45524	ESO575-061	AGC029274	1649	165	17	5.0	2.94	1649	168
J130947-101916	45652	PGC045652	HIPASSJ1309-10	1206	207	16	5.8	14.02	1210	196
J131035-214450	45721	ESO576-003	AGC029327 shg05	2959	231	16	6.6	11.27	2962	238
J131305-195830	45911	ESO576-011	AGC029361	2757	309	11	12.4	13.23	2759	306
J131321-185558	45935	ESO576-012	AGC029366 shg05	6148	235	17	4.9	3.19	6149	237
J131330-193244	45952	NGC5022	AGC029371	3001	392	18	4.3	8.46	3005	398
J131334-152553	45958	PGC045958	HIPASSJ1313-15	2503	81	15	7.9	12.19	2501	73
J131702-104612	46252	IC4216	HIPASSJ1316-10	2839	257	16	5.9	7.06	2838	263
J131706-161516	46261	PGC046261	AGC530085 shg05	2631	288	19	2.9	8.27	2636	279
J131739-213708	46299	ESO576-023	AGC029435 shg05	2947	188	25	2.7	6.34	2933	124
J131835-211758	46373	ESO576-026	AGC029453	1953	163	18	3.9	2.40	1955	181
J131920-145037	46441	NGC5073	AGC530097 shg05	2745	385	15	8.0	16.07	2746	405
J131934-124159	46473	NGC5079	AGC530104	2228	235	16	6.6	1.92	2223	249
J132018-214925	46525	NGC5084	HIPASSJ1320-21	1719	662	100	8.7	102.72	1719	655
J132148-131222	46664	NGC5105	AGC530120 shg05	2903	219	12	11.1	14.30	2903	220
J132430-210729	46878	IC4237	AGC029585 shg05	2667	325	18	3.8	14.03	2607	205
J132441-194214	46889	ESO576-050	AGC029590	1969	189	14	8.7	17.01	1967	192
J132500-240035	46920	ESO508-071	AGC029599 shg05	7378	315	18	4.5	3.14	7388	319
J133017-214446	47450	ESO576-072	AGC029740	7314	228	100	5.6	2.45	7312	248
J133058-215044	47505	ESO577-001	AGC029757	7361	379	100	3.4	4.35	7366	371
J133103-150604	47514	PGC047514	AGC530277 shg05	4232	300	18	4.2	6.22	4231	303
J133208-225710	47599	ESO509-045	AGC029792	5047	278	19	2.8	3.20	5056	266
J133209-245132	47600	ESO509-044	AGC029789	7791	450	100	2.8	4.09	7790	439
J133314-160715	47717	PGC047717	tmc06	6342	206	100	3.4	2.35	6120	683
J133933-222957	48300	ESO577-020	AGC029955 shg05	6998	249	19	2.7	2.67	7000	235
J133949-221815	48323	ESO577-022	AGC029961	5760	285	17	4.7	2.62	5746	302
J134002-252831	48346	IC4315	AGC029965	5163	322	50	3.8	3.10	5134	303

shg05 = Springob et al. (2005)

ctf09 = Courtois et al. (2009)

tmc06 = Theureau et al. (2006)

APPENDIX

A01 SoFiA velocity widths

In addition to the velocity widths we have measured and presented in Table 3, the SoFiA pipeline for WALLABY provides Wm50⁹, and the relation between the two is shown in Figure A1. Both are HI profile widths at 50%, but there is a systematic difference which is mostly unrelated to signal-to-noise. Both velocity widths are from velocities on the optical convention. A linear fit has a slope of 0.92 and a χ^2 of 1.3. In other words, the scatter is close to that expected on the grounds of measurement errors, but the non-unity slope is a quantity to be noted for investigations that require a calibrated TFR. The mean difference W50 – Wm50 is -7.7 ± 0.7 km s⁻¹ with no significant difference in the mean between the high and lower SNR data. We use our measured W50s in this paper, because measurement errors are computed. Not so for Wm50.

The Wm50 measurements are made by interpolating the WALLABY spectrum at 50% of the peak flux. This is automated. The w50 values on the other hand are measured by isolating the region of the spectrum where the galaxy flux is by setting a cursor. Based on the signal to noise a level of smoothing is chosen (2, 4, 8 pixels), and the smoothed spectrum is then interpolated similarly. The conversion of w50 to Wmx takes account of the broadening introduced by this smoothing. For the full WALLABY survey it may be necessary to adopt the Wm50 approach. But it will be important to include uncertainty calculation in the process.

A02 Alternative axial ratios

In §3.2 we compared IRAF measurements of axial ratios on *g* band DECaLS images with kinematic inclinations. The comparison showed considerable scatter. Other sources of inclinations are worthy of consideration and we show them in Figure A2. The measurement of WISE total magnitudes also produces axial ratios and these are shown in red in the figure. They are biased towards higher inclinations than the kinematic inclinations. We also wrote an ellipse fitting program on a different principle from that of the IRAF task aiming at the 25th *g* magnitude isophote. Minimization of the deviation from an ellipse with (*a*, *b*, & PA) as the parameters of the isophotal pixels yields the solid black symbols with error bars in Figure A2. The horizontal axis errors derive from the covariance matrix of the fit. They seem unrealistically small, but, while some inclined TFR galaxies are well fitted by ellipses in the outer disk, others are more irregular in their stellar light distribution, a problem acknowledged in the original TFR paper (Tully & Fisher 1977). These inclinations are also biased towards higher inclinations, which the IRAF inclinations (Figure 13) are not.

The SoFiA source finding algorithm also provides estimates of *a* and *b* for the neutral hydrogen. Inclinations from this axial ratio are plotted in blue, the solid symbols for the raw *b/a*, the open symbols for the same galaxies after subtracting 5 pixels in quadrature to allow for the WALLABY beam size. The raw values are biased, but the open ones, which are not biased, have more scatter. The sample with kinematic

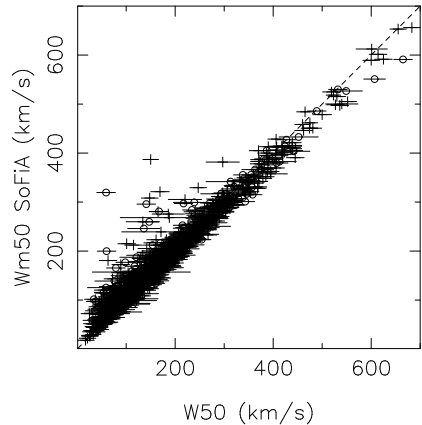
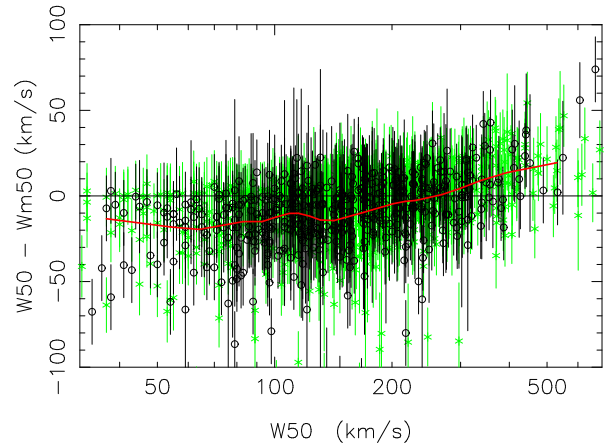


Figure A1. Comparison of SoFiA Wm50s with those in Table 3 for the NGC 5044 field. Crosses are for S/N > 3, open circles for S/N < 3. The figure below shows the differences, with the higher S/N in green. The red line is a running mean.



models is still small and will remain only a subset of WALLABY TFR galaxies. However, it is possible that bias in the raw hydrogen axial ratios can be calibrated out, when more data are available. This might be the path to dispensing with troublesome optical inclinations.

Finally, the stack of galaxies in Figure A2 at 90° axial ratio inclinations is due to galaxies being measured with *b/a* < 0.2. This choice of minimum axial ratio should be revised when more data are obtained. For the time being we note that $-8.7 \log \sin 80^\circ = 0.06$ mag, a small correction.

A03 CosmicFlows4 distances

The positions of WALLABY galaxies within the Cosmic Web can be studied using the full matter (dark and luminous) density contrast field (usually denoted δ) reconstructed from the CosmicFlows- 4 Catalogue of peculiar velocities (Tully

⁹ This is distinct from w50 in the WALLABY catalogue.

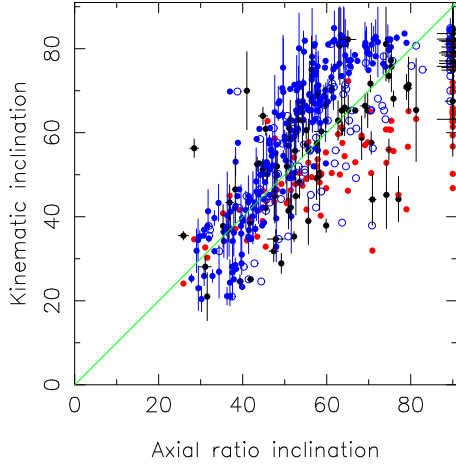


Figure A2. Alternative sources of disk inclination. Solid black symbols are from ellipse fitting to g band with experimental software; the red symbols are from WISE W1 axial ratios; the blue symbols are from resolved WALLABY hydrogen maps (open, with beam size correction), (solid, without). All these are plotted against kinematic inclinations by Deg et al. (2022). Pilot survey phase 1 data have been included in the solid blue category to more fully populate the graph, and these have error bars to distinguish them.

et al. 2023, Courtois et al. 2023). This catalogue now uses the Baryonic TFR (Kourkchi et al. 2022) to calculate distances, and stellar masses are obtained from multiwavelength photometry. Our WALLABY galaxies have W1 photometry, although within the decade multiwavelength galaxy photometry may be supplied by the Rubin Telescope. For the 10,000 CF4 galaxies we have compared baryonic masses calculated with stellar masses from W1 as in §2.4 with those published in CF4. The result is in Figure A3, after a correction of 0.525 mag to the W1 magnitudes of Kourkchi et al. , which are from a different source from the W1 total magnitudes used here and in Paper 1. This allows us to use a baryonic TFR calibration relation from the adjusted CF4 galaxies, shown in Figure A4. To be incorporated into CosmicFlows4, the distance moduli obtained with this calibration also needed a 0.15 mag change for the Hubble constant used in this paper and that calculated from the CF4 database.

A04 Siena catalogue TFR for the NGC4808 field

The Siena catalogue (Moustakas et al. 2023) has photometry in the grz bandpasses for bright galaxies over half the sky and aspires to complete sky coverage outside the Galactic plane. These total magnitudes are measured by exponential disk fitting which also produces axial ratios. We show the TFR in the NGC 4808 field for z magnitudes and Siena axial ratios in Figure A5. The normal cut is applied to inclinations, but no S/N cut is made. This is a promising new resource for the WALLABY project.

This paper has been typeset from a $\text{\TeX}/\text{\LaTeX}$ file prepared by the author.

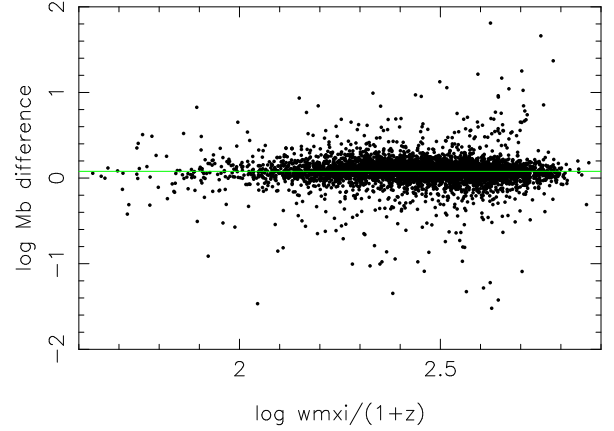


Figure A3. Difference in baryonic mass calculated with W1 magnitudes only and with the multiwavelength photometry of Kourkchi et al. (2022).

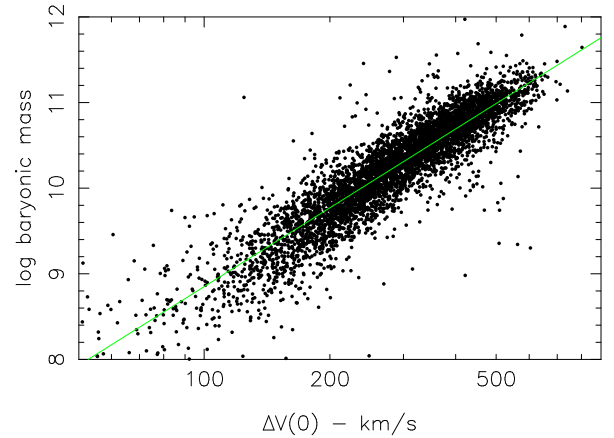


Figure A4. The calibration used in §5.3 for the baryonic TFR, based on the CF4 galaxies of Kourkchi et al. (2022).

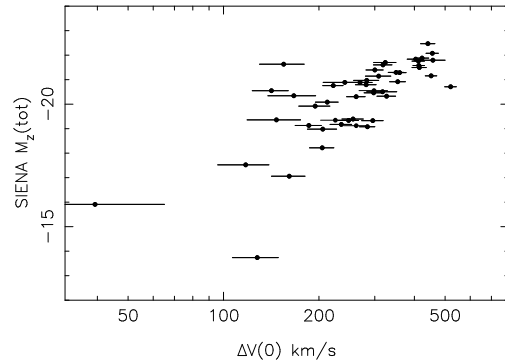


Figure A5. The TFR for the NGC4808 field from Siena catalogue z band photometry. These magnitudes are on the AB system.